Author(s): Vaparanta, Katri; Jokilammi, Anne; Paatero, Ilkka; Merilahti, Johannes A.; Heliste, Juho; Hemanthakumar, Karthik Amudhala; Kivelä, Riikka; Alitalo, Kari; Taimen, Pekka; Elenius, Klaus

Title: STAT5b is a key effector of NRG-1/ERBB4-mediated myocardial growth

Year: 2023

Version: Published version

Vaparanta, K., Jokilammi, A., Paatero, I., Merilahti, J. A., Heliste, J., Hemanthakumar, K. A., Kivelä, R., Alitalo, K., Taimen, P., & Elenius, K. (2023). STAT5b is a key effector of NRG-1/ERBB4-mediated myocardial growth. Embo reports, 24(5), Article e56689. https://doi.org/10.15252/embr.202256689

Article

SOURCE DATA | TRANSPARENT PROCESS | OPEN ACCESS

EMBO reports

STAT5b is a key effector of NRG-1/ERBB4-mediated myocardial growth

Katri Vaparanta[1,2,3], Anne Jokilammi[1,2,3], Ilkka Paatero[1], Johannes A Merilahti[1], Juho Heliste[1,2,3], Karthik Amudhala Hemanthakumar[4,5], Riikka Kivelä[4,5,6], Kari Alitalo[4,5], Pekka Taimen[7,8] & Klaus Elenius[1,2,3,9,*]

Abstract

The growth factor Neuregulin-1 (NRG-1) regulates myocardial growth and is currently under clinical investigation as a treatment for heart failure. Here, we demonstrate in several *in vitro* and *in vivo* models that STAT5b mediates NRG-1/EBBB4-stimulated cardiomyocyte growth. Genetic and chemical disruption of the NRG-1/ERBB4 pathway reduces STAT5b activation and transcription of STAT5b target genes *Igf1*, *Myc*, and *Cdkn1a* in murine cardiomyocytes. Loss of *Stat5b* also ablates NRG-1-induced cardiomyocyte hypertrophy. Dynamin-2 is shown to control the cell surface localization of ERBB4 and chemical inhibition of Dynamin-2 downregulates STAT5b activation and cardiomyocyte hypertrophy. In zebrafish embryos, Stat5 is activated during NRG-1-induced hyperplastic myocardial growth, and chemical inhibition of the Nrg-1/Erbb4 pathway or Dynamin-2 leads to loss of myocardial growth and Stat5 activation. Moreover, CRISPR/Cas9-mediated knockdown of *stat5b* results in reduced myocardial growth and cardiac function. Finally, the NRG-1/ERBB4/STAT5b signaling pathway is differentially regulated at mRNA and protein levels in the myocardium of patients with pathological cardiac hypertrophy as compared to control human subjects, consistent with a role of the NRG-1/ERBB4/STAT5b pathway in myocardial growth.

Keywords cardiomyocyte hyperplasia; cardiomyocyte hypertrophy; dynamin; NRG-1–ErbB pathway; signal transducer and activator of transcription
Subject Categories Cardiovascular System; Signal Transduction
DOI 10.15252/embr.202256689 | Received 18 December 2022 | Revised 7 March 2023 | Accepted 10 March 2023 | Published online 3 April 2023
EMBO Reports (2023) 24: e56689

Introduction

Neuregulin-1 (NRG-1) has been implicated as a central regulator of both hypertrophic and hyperplastic cardiomyocyte growth (Zhao *et al*, 1998; Baliga *et al*, 1999; Bersell *et al*, 2009). Neuregulin-1 is synthesized in cardiac endothelial cells (Lemmens *et al*, 2006; Hedhli *et al*, 2011) and released from the cell surface of endothelial cells mainly by the ADAM-17 protease (Montero *et al*, 2000). The release of NRG-1 has been reported to be induced by angiogenic factors through the VEGFR2 receptor (Kivelä *et al*, 2019). Neuregulin-1 activates ERBB receptor tyrosine kinases by inducing their dimerization and subsequential transphosphorylation, and is known to signal through the ERBB2/ERBB4 heterodimer in the myocardium (Gassmann *et al*, 1995; Lee *et al*, 1995; Meyer & Birchmeier, 1995). Of these two ERBB receptors, only ERBB4 can directly bind NRG-1. ERBB2 is activated by dimerizing with the NRG-1-bound ERBB4 receptor (Plowman *et al*, 1993). Genetic knockout or chemical inhibition of NRG-1, ERBB2, or ERBB4 in mouse models has been shown to lead to a distinct heart phenotype during embryogenesis characterized by dilated ventricles, thin ventricular walls and loss of trabeculae (Gassmann *et al*, 1995; Lee *et al*, 1995; Meyer & Birchmeier, 1995), and to dilated cardiomyopathy in the adulthood (Crone *et al*, 2002; Özcelik *et al*, 2002; García-Rivello *et al*, 2005). A similar heart phenotype has also been observed in zebrafish embryos expressing a mutant *erbb2* transgene or a protein trap for the Erbb4 ligand Nrg2a, as well as in larvae treated with chemical inhibitor of the Erbb2/Erbb4 heterodimer (Liu *et al*, 2010; Rasouli & Stainier, 2017). Moreover, overexpression of Nrg-1 or constitutively active ERBB2 has been reported to lead to cardiomegaly in adult zebrafish and in neonatal and adult mice models, respectively (D'uva *et al*, 2015; Gemberling *et al*, 2015). After injury, NRG-1 promotes regeneration of the heart by inducing proliferation of cardiomyocytes both in adult mice and in adult zebrafish (Bersell

1 Turku Bioscience Centre, University of Turku and Åbo Akademi University, Turku, Finland
2 Medicity Research Laboratories, University of Turku, Turku, Finland
3 Institute of Biomedicine, University of Turku, Turku, Finland
4 Wihuri Research Institute, Helsinki, Finland
5 Translational Cancer Biology Program, Research Programs Unit, Faculty of Medicine, University of Helsinki, Helsinki, Finland
6 Faculty of Sport and Health Sciences, University of Jyväskylä, Jyväskylä, Finland
7 Institute of Biomedicine and FICAN West Cancer Centre, University of Turku, Turku, Finland
8 Department of Pathology, Turku University Hospital, Turku, Finland
9 Department of Oncology, Turku University Hospital, Turku, Finland
*Corresponding author. Tel: +358 50 514 2307; E-mail: klaus.elenius@utu.fi
The copyright line for this article was changed on 21 June 2023 after original online publication.

et al, 2009; Gemberling et al, 2015). In several injury mouse models, administration of recombinant NRG-1 has attenuated cardiac injury (Odiete et al, 2012; Mendes-Ferreira et al, 2013). Therefore, after successful phase II trials (Gao et al, 2010; Jabbour et al, 2011), NRG-1 is currently tested in phase III clinical trials as a treatment for heart failure (Gao et al, 2018; Zensun Sci. & Tech. Co., Ltd., 2018) .

The NRG-1/ERBB pathway has been shown to activate PI3K/AKT, MAPK, and SRC/FAK pathways in cardiomyocytes (Baliga et al, 1999; Fukazawa et al, 2003; Kuramochi et al, 2006; Jie et al, 2012; Cai et al, 2016; Pentassuglia et al, 2016), none of which has been demonstrated to directly control NRG-1/ERBB-mediated cardiomyocyte growth in *in vitro* or *in vivo* settings. Instead, the PI3K/AKT pathway has been affiliated with cardiomyocyte survival, DNA synthesis and glucose uptake (Fukazawa et al, 2003; Bersell et al, 2009; Jie et al, 2012; Pentassuglia et al, 2016), the MAPK pathway with protein synthesis and sarcomere organization (Baliga et al, 1999), and the SRC/FAK pathway with cytoskeletal remodeling (Kuramochi et al, 2006).

In our previous study, we discovered that the transcription factor STAT5b is selectively activated by the JM-b isoform of ERBB4 (Vaparanta et al, 2022), the ERBB4 isoform preferentially expressed by cardiomyocytes (Fig EV1A) (Elenius et al, 1997; Wang et al, 2021). Of the two *STAT5* genes, *STAT5b* is also the major *STAT5* gene expressed in the heart both at mRNA and at protein level (Fig EV1B). Since chemical inhibition of STAT5 has previously been shown to attenuate myocardial growth induced by angiotensin II (Jin et al, 2022) or by pressure overload in mice (Kimura et al, 2018), we set out to explore the role of STAT5b in NRG1/ERBB4-mediated myocardial growth. As NRG-1 has been reported to induce both hypertrophic growth in neonatal and adult cardiomyocytes as well as hyperplastic growth in embryonic cardiomyocytes (Zhao et al, 1998), we employed both adult and neonatal murine and embryonic zebrafish models to investigate the role of STAT5b in NRG-1/ERBB4-induced cardiac growth. Clinical human samples were examined to investigate whether the hypothesized signaling pathway is active also in human in states of increased myocardium growth. The analyses validated in both *in vitro* and *in vivo* models demonstrated that the NRG-1 receptor ERBB4, the ERBB4-activated intracellular signaling molecule STAT5b, and the ERBB4 trafficking-regulator dynamin-2 mediate both hypertrophic and hyperplastic NRG-1-induced cardiomyocyte growth. In addition, we discovered altered signaling of the NRG-1/ERBB4/STAT5b/dynamin-2 pathway in the myocardia of patients suffering from pathological cardiac hypertrophy.

Results

NRG-1/ERBB4 pathway controls STAT5b signaling *in vivo* in adult murine heart

To explore the role of STAT5b in ERBB4-mediated hypertrophic myocardial growth, mice expressing the soluble ectodomain (ECD) of ERBB4 in the heart as a result of infection with an adeno-associated virus of serotype 9 carrying the mouse ERBB4 ECD insert (AAV9-mERBB4ECD) were utilized. The ERBB4 ECD traps ERBB4 ligands, such as NRG-1, leading to downregulation of ERBB4 signaling in the cardiomyocytes (Kivelä et al, 2019).

First, the effect of AAV9-mERBB4ECD treatment on cardiomyocyte size was assessed to learn whether reduction in ERBB4-sensitive signaling is associated with cardiomyocyte growth. The cardiomyocyte thickness was determined from heart sections (Fig 1A and B). As expected, the average cardiomyocyte thickness was lesser in the AAV9-mERBB4ECD-treated mice as compared to the controls (Fig 1A and B).

The activation of STAT5b by phosphorylation in the key tyrosine residue 699 leads to STAT5b dimerization and consequential accumulation into the nucleus at the target gene transcription sites. To explore the role of ErbB4 ligands in STAT5b activation in cardiomyocytes, the nuclear accumulation of STAT5b in the AAV9-mERBB4ECD and AAV9-control treated hearts was addressed by immunostaining (Fig 1C and D). The nuclear accumulation of STAT5b was found to be reduced in the AAV9-mERBB4ECD-treated hearts as compared to the controls, indicating a role for ERBB4 ligands in STAT5b activation in cardiomyocytes (Fig 1C and D).

The effect of the AAV9-mERBB4ECD-treatment on the transcription of known STAT5b target genes was further assessed with real-time RT-PCR (Fig 1E). The treatment with AAV9-mERBB4ECD significantly decreased the levels of *Igf1* and *Myc* transcripts (Fig 1E), both of which are encoded by known STAT5b target genes that have been found to promote cardiac hypertrophy *in vivo* (Delaughter et al, 1999; Nosaka et al, 1999; Lord et al, 2000; Zhong et al, 2006; Basham et al, 2008; Rotwein, 2012). In addition to *Igf1* and *Myc*, the transcription of a third STAT5b target gene, *Cdkn1a* (Yu et al, 2010), was similarly decreased.

NRG-1/ERBB4 pathway controls STAT5b signaling *in vitro* in neonatal murine cardiomyocytes

To explore the STAT5b-dependency of NRG-1/ERBB4-mediated cardiomyocyte growth, cardiomyocytes from neonatal mice were isolated. As expected, the primary cardiomyocytes expressed ERBB4 JM-b more than the JM-a isoform (Fig EV1C) were positive for cardiomyocyte lineage-specific markers myosin-heavy-chain and tropomyosin (Fig EV1D), and exhibited sporadic contractions in the culture plate. To assess the effect of STAT5b knockdown on NRG-1-induced cardiomyocyte hypertrophy, the isolated cardiomyocytes were infected with lentiviral particles containing plasmids encoding *Stat5b*-targeting shRNAs or control shRNA (Fig EV1E) and stimulated or not with NRG-1 for 2 days. The cardiomyocytes were stained with an antibody recognizing the heavy chain of a skeletal and cardiac myocyte specific myosin II, analyzed with immunofluorescence, and the cross-sectional area of the cardiomyocytes was quantified from confocal images taken in plane with the plasma membrane. The *Stat5b* knockdown significantly reduced the hypertrophic response induced by NRG-1 (Fig 1F and G), suggesting that NRG-1-stimulated hypertrophy is at least partially dependent on STAT5b.

To address the role of ERBB4 as a receptor for NRG-1 in mediating the hypertrophic response, *Erbb4* was knocked down in mouse primary cardiomyocytes by RNA interference (Fig EV1F–H). The treatment with *Erbb4*-targeting shRNAs significantly reduced the nuclear accumulation of STAT5b, as well as the cross-sectional area of cardiomyocytes (Fig 1H and I). To confirm that the transcription of STAT5b target genes in cardiomyocytes was STAT5b- and ERBB4-dependent, expression of *Igf1*, *Myc*, and *Cdkn1a* was

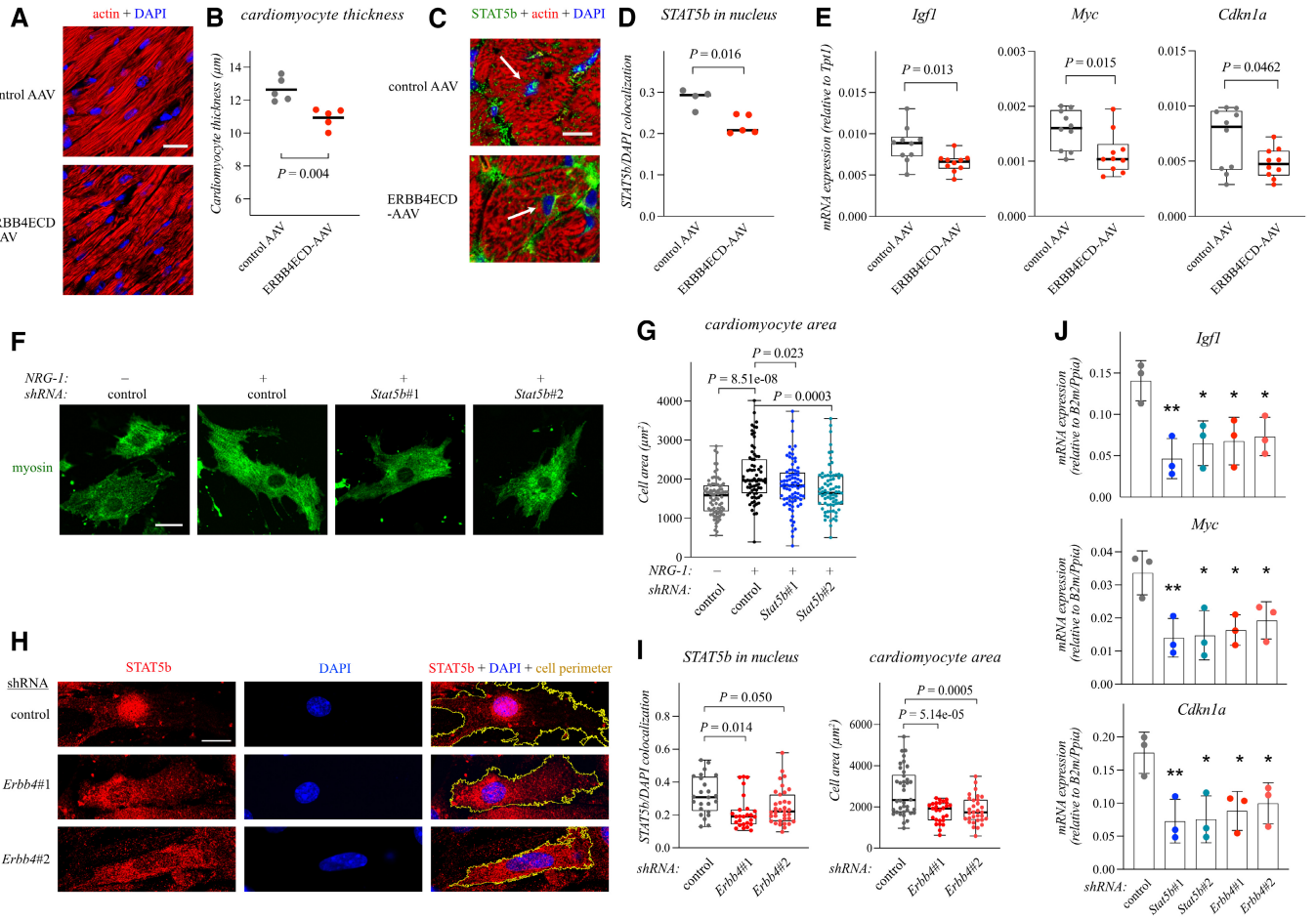

Figure 1. NRG-1 promotes cardiomyocyte hypertrophy via ERBB4 and STAT5b.

A, B Confocal images (A) and quantification (B) of immunofluorescence staining of actin filaments (phalloidin) and nuclei (DAPI) in cardiomyocytes. Images of cryosections from hearts of mice transduced with either control (control AAV) or ERBB4 ectodomain-encoding (ERBB4ECD-AAV) adeno-associated viruses are shown. One dot in the scatterplot corresponds to the average cardiomyocyte thickness as defined by the thickness of the myofibril bundle per cardiomyocyte in 3–5 randomly acquired images of stained sections from one heart (for each group $n = 5$, biological replicates). Two-tailed unpaired *T*-test was used for statistics. Scale bar 20 µm.

C, D Confocal images (C) and quantification (D) of immunofluorescence staining of STAT5b, actin filaments (phalloidin) and nuclei (DAPI) in cardiomyocytes of cryosections from the hearts of mice transduced with either control- or ERBB4ECD-AAV. Panel D depicts quantification of colocalization of STAT5b- and DAPI-specific signals. One dot in the boxplot corresponds to the median value in 20–50 images of stained sections from one heart (control AAV: $n = 4$, ERBB4ECD-AAV: $n = 5$, biological replicates). Two-tailed unpaired *T*-test was used for statistics. Scale bar 10 µm. White arrows point to cardiomyocyte nuclei.

E Real-time RT-PCR analysis of expression of the indicated STAT5b target genes in the heart of mice transduced with either control- or ERBB4ECD-AAV. One dot corresponds to analysis of one heart ($n = 10$; biological replicates combined from two replicate experiments). Two-tailed unpaired *T*-test was used for statistics.

F, G Confocal images (F) and quantification (G) of immunofluorescence staining of myosin heavy chain in primary mouse cardiomyocytes. The cells were treated with either control or *Stat5b*-targeting shRNAs and stimulated with NRG-1 for 2 days. Myosin immunoreactivity was used to quantify cell area. One dot in the boxplot corresponds to one cell (Control no NRG-1: $n = 83$, control with NRG1: $n = 73$, Stat5b#1 with NRG-1: $n = 80$, Stat5b#2 with NRG1: $n = 75$; technical replicates combined from four biological replicate experiments). Non-parametric Kruskal-Wallis ANOVA was used. *Post hoc* analyses were conducted with the Mann Whitney *U*-test and the resulting *P*-values were corrected with the method of Benjamini, Krieger and Yekutieli. Scale bar 20 µm.

H, I Confocal images (H) and quantification (I) of immunofluorescence staining of STAT5b and nuclei (DAPI) in mouse cardiomyocytes. The cells were treated with either control or *Erbb4*-targeting shRNAs. Panel I depicts quantification of colocalization of STAT5b- and DAPI-specific signals (left) and the cell perimeter (right). One dot in the boxplots corresponds to one cell (Control: $n = 24$, Erbb4#1: $n = 26$, Erbb4#2: $n = 35$; technical replicates combined from two biological replicate experiments). Non-parametric Kruskal-Wallis ANOVA and Dunn's multicomparison test (colocalization analysis) and Brown-Forsythe one-way ANOVA and Dunnett's multicomparison test (cardiomyocyte size analysis) with multiple test correction were used for statistics. Scale bar 20 µm.

J Real-time RT-PCR analysis of expression of the indicated STAT5b target genes in mouse cardiomyocytes. The cells were treated with either control, *Stat5b*- or *Erbb4*-targeting shRNAs and stimulated with NRG-1 for 30 min. One dot corresponds to the mean of technical replicates in one experiment and the whiskers the standard deviation (for each group $n = 3$; biological replicate experiments). One-way ANOVA and the Dunnett's multicomparison test with multiple test correction was used for statistics. $*P \leq 0.05$; $**P < 0.01$; $***P < 0.001$ against control shRNA (*Igf-1* panel: Stat5b#1 $P = 0.0038$, Stat5b#2 $P = 0.0153$, Erbb4#1 $P = 0.0188$, Erbb4#2 $P = 0.0288$; *Myc* panel: Stat5b#1 $P = 0.0093$, Stat5b#2 $P = 0.0119$, Erbb4#1 $P = 0.0197$, Erbb4#2 $P = 0.0512$; *Cdkn1a* panel: Stat5b#1 $P = 0.0091$, Stat5b#2 $P = 0.0107$, Erbb4#1 $P = 0.0235$, Erbb4#2 $P = 0.048$).

Data information: For all boxplots the central band represents the median, the box the interquartile range and whiskers the whole range of values.
Source data are available online for this figure.

analyzed in cells subjected to *Stat5b* or *Erbb4* knockdown after stimulating the cells for 30 min with NRG-1. Real-time RT-PCR analyses demonstrated that both *Stat5b- and Erbb4-targeting* shRNAs significantly downregulated the expression of all three STAT5b target genes (Fig 1J). Taken together, these results demonstrate that the loss of NRG-1/ERBB4 signaling correlates with the loss of STAT5b signaling and reduced cardiomyocyte size in murine cardiomyocytes.

Dynamin-2 controls subcellular ERBB4 localization and STAT5b activation in neonatal murine cardiomyocytes

Mass spectrometry-derived ERBB4 interactome indicated that dynamin-2 (encoded by *DNM2* gene) was one of the prominent interaction partners of ERBB4 (Fig EV2A). Experimentation with proximity ligation assay (PLA) suggested that the heart-specific ERBB4 JM-b isoform was more prone to associate with dynamin-2 than the alternative isoform ERBB4 JM-a (Fig EV2B and C). The interaction between dynamin-2 and ERBB4 may have implications for heart biology, since the loss of *dnm2* has been, similarly to the loss of *Nrg1* and *Erbb4*, associated with the development of heart failure (Li *et al*, 2013). Previous research also indicates that the dynamin GTPases control vesicular endocytotic and ER-to-golgi trafficking. Of the three genes encoding dynamins, *DNM2* is most abundantly expressed in the heart both at mRNA and at protein level (Fig EV2D; Li *et al*, 2013).

To test whether ERBB4 interacts with Dynamin-2 in cardiomyocytes, the association between the two proteins was addressed with PLA in primary murine cardiomyocytes. In addition, to analyze whether the interaction was dependent on the Dynamin-2 GTPase activity, the cardiomyocytes were cultured in the presence or absence of the Dynamin GTPase inhibitor dynasore. ERBB4 and Dynamin-2 indeed associated with each other in both control- and dynasore-treated cardiomyocytes (Fig 2A and B). Treatment with dynasore, however, significantly affected the subcellular localization of the associations between endogenously expressed ERBB4 and Dynamin-2. Dynasore selectively reduced the associations at the cell surface and periphery of the cardiomyocytes (Fig 2C and D).

To further explore the effect of Dynamin inhibition on ERBB4 location, ERBB4 isoforms expressed in MCF-7 cells were analyzed for colocalization with the plasma membrane marker Na-K ATPase after treatment with dynasore or the control buffer. Dynasore significantly reduced the colocalization of both ERBB4 JM-a and JM-b isoforms with Na-K ATPase at the cell surface, indicating that the cell surface localization of ERBB4 was specifically dependent on the GTPase activity of Dynamin-2 (Fig EV2E and F).

To explore whether the effect of dynamin-2 on ERBB4 localization was reflected in the downstream signaling via STAT5b, ERBB4 JM-b was overexpressed in mammary epithelial cells treated with dynasore or *DNM2*-targeting siRNAs. Both treatments abolished ERBB4 overexpression-promoted phosphorylation of the activating residue of STAT5b (Fig EV2G and H) and dynasore treatment additionally disrupted the co-precipitation of ERBB4 JM-b with STAT5b (Fig EV2I). Moreover, nuclear accumulation of STAT5b was reduced in cardiomyocytes treated with dynasore (Fig 2E and F), and both a chemical ERBB inhibitor AG1478 as well as dynasore significantly reduced the NRG-1-stimulated expression of STAT5b target genes (Fig 2G).

To control that the inhibition of the GTPase activity of dynamin-2 also affected the NRG-1-stimulated hypertrophic response, dynasore-treated cardiomyocytes were stimulated with NRG-1 for 2 days and analyzed for cross-sectional area. The area was significantly reduced by dynasore (Fig 2H and I). Taken together, the results indicate that Dynamin-2 regulates subcellular ERBB4

Figure 2. Dynamin-2 controls ERBB4 signaling and cardiomyocyte hypertrophy.

A, B Proximity ligation assay (PLA) of association of Dynamin-2 with ERBB4 in primary mouse cardiomyocytes treated with either DMSO or the dynamin inhibitor dynasore for 5 h. Panel A depicts a z projection of a stack of confocal images. PLA interactions are shown in red, nuclear stain DAPI in blue. Panel B depicts quantification of the data. One dot in the boxplot corresponds to the number of PLA signals in μm^2 in one cell (Control: $n = 6$, DMSO buffer: $n = 11$, dynasore: $n = 11$; technical replicates from one of two biological replicate experiments). Non-parametric Kruskal-Wallis ANOVA and the Dunn's multicomparison test with multiple test correction was used for statistics. Scale bar 20 μm.

C, D Analysis of the subcellular localization of the association of Dynamin-2 with ERBB4. Panel C depicts Dynamin-2/ERBB4 PLA interactions in blue in representative cells (tracked) as well as when the PLA signals were artificially randomly distributed throughout the area of the cell (randomized). Panel D depicts quantification of the PLA interactions within 1 μm distance from the edges of the cells (cell periphery). One dot in the boxplot corresponds to the fraction of PLA signals in the cell periphery in one cardiomyocyte (for each group $n = 12$; technical replicates combined from two biological replicate experiments). Non-parametric Mann–Whitney *U*-test was used for statistics. Scale bar 20 μm.

E, F Confocal images I and quantification (F) of immunofluorescence staining of STAT5b and the nuclear stain DAPI in primary mouse cardiomyocytes. The cells were treated with either DMSO or dynasore for 5 h and stimulated for 15 min with NRG-1. Panel (F) depicts quantification of colocalization of STAT5b- and DAPI-specific signals. One dot in the boxplots corresponds to one cell (DMSO: $n = 15$, dynasore: $n = 19$; technical replicates combined from two biological replicate experiments). Non-parametric Mann–Whitney *U*-test was used for statistics. Scale bar 20 μm.

G Real-time RT-PCR analysis of expression of the indicated STAT5b target genes in primary mouse cardiomyocytes treated for 1–3 h with the DMSO buffer, the ERBB kinase inhibitor AG1478, or dynasore, and stimulated or not for 30 min with NRG-1. One dot corresponds to the mean of technical replicates in one experiment and the whiskers the standard deviation (for each group in *Igf-1* and *Cdkn1a* panel: $n = 6$, for each group expect the dynasore group in *Myc* panel: $n = 4$, for the dynasore group in *Myc* panel: $n = 3$; biological replicate experiments). One-way ANOVA and the Dunnett's multicomparison test with multiple test correction was used for statistics. $^*P < 0.05$; $^{**}P < 0.01$; $^{***}P < 0.001$; against DMSO + NRG-1 treatment (*Igf-1* panel: DMSO without NRG-1 $P = 0.0041$, AG1478 $P = 0.0082$, dynasore $P = 6.61e\text{-}06$; *Myc* panel: DMSO without NRG-1 $P = 0.0386$, AG1478 $P = 0.0037$, dynasore $P = 0.0064$; *Cdkn1a* panel: DMSO without NRG-1 $P = 0.0123$, AG1478 $P = 0.0064$, dynasore $P = 0.0092$).

H, I Confocal images (H) and quantification (I) of immunofluorescence staining of myosin heavy chain in primary mouse cardiomyocytes. The cells were treated with either DMSO or dynasore and stimulated with NRG-1 for 2 days. The myosin immunoreactivity was used to quantify cell area. One dot in the boxplot corresponds to one cell (DMSO: $n = 22$, dynasore: $n = 28$; technical replicates combined from three biological replicate experiments). Non-parametric Mann–Whitney *U*-test was used for statistics. Scale bar 20 μm.

Data information: For all boxplots the central band represents the median, the box the interquartile range and whiskers the whole range of values.
Source data are available online for this figure.

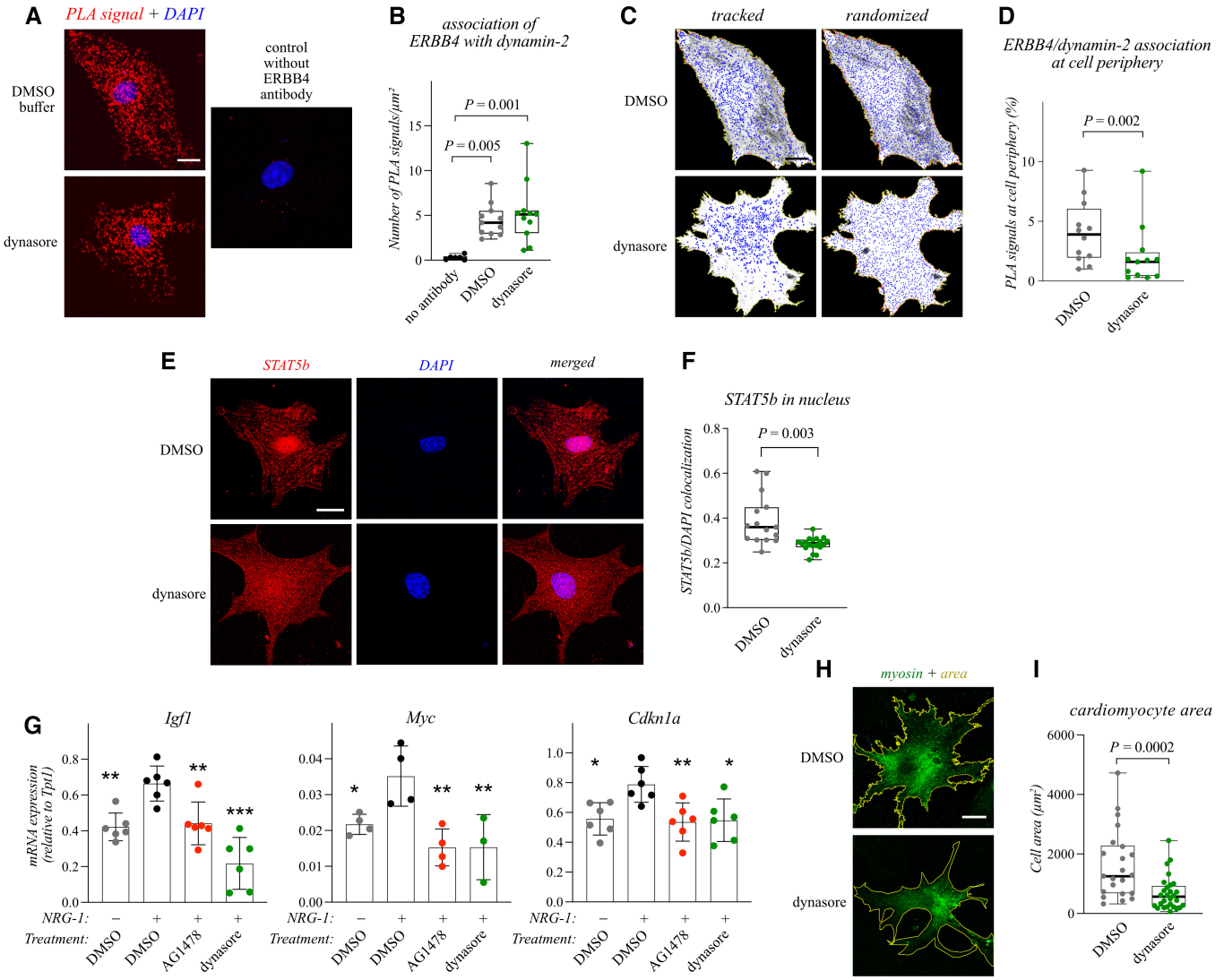

Figure 2.

localization and, consequently, NRG-1-stimulated STAT5b activation and cardiomyocyte growth.

NRG-1 activates Stat5 in embryonic zebrafish model of hyperplastic myocardial growth *in vivo*

In addition to hypertrophic growth, NRG-1/ERBB signaling has been reported to induce hyperplastic myocardial growth in zebrafish models and in embryonic mice (Zhao *et al*, 1998; Liu *et al*, 2010; Gemberling *et al*, 2015). To explore the role of STAT5b also in the context of NRG-1-induced hyperplastic growth, human recombinant NRG-1 or the control substance (BSA) was injected into the pericardial cavity of zebrafish embryos at 2 days post fertilization (dpf). The embryos were fixed at 4 dpf and stained with a myosin heavy chain antibody to visualize the myocardium. The cross-sectional ventricular area and ventricle thickness were measured from confocal images taken from anterior cross sections of the ventricles. The NRG-1 injection induced hyperplastic cardiomyocyte growth as indicated by the increase in cross-sectional ventricular area but not in ventricular wall thickness (Fig 3A–D). This was further confirmed by assessing the ratio of the amount of nuclei in the ventricle to the ventricular area of the NRG-1-injected and BSA-injected embryos (Fig 3A and B). An increase in the number of nuclei in the myocardium of NRG-1-injected embryos was observed indicating proliferative growth.

The effect of NRG-1 injection to the cardiac function of the zebrafish embryos was further assessed with live imaging (Fig 3E and F, Movies EV1 and EV2). The ventricles of the NRG-1-injected and BSA-injected zebrafish demonstrated similar ejection fractions indicating that the NRG-1 induced hyperplastic growth was physiological.

To assess the signaling pathways activated by the NRG-1 injections, western analyses were performed (Fig 3G and H). Unsurprisingly, the Pi3k/Akt and Erk pathways were activated with NRG-1. In addition, the Stat5 pathway was activated as indicated by the increased phosphorylation in the activating residue of the zebrafish Stat5 (Fig 3G and H). While the phosphospecific antibody does not differentiate between the zebrafish Stat5a and Stat5b, it is of note that both zebrafish Stat5a and Stat5b share more sequence similarity

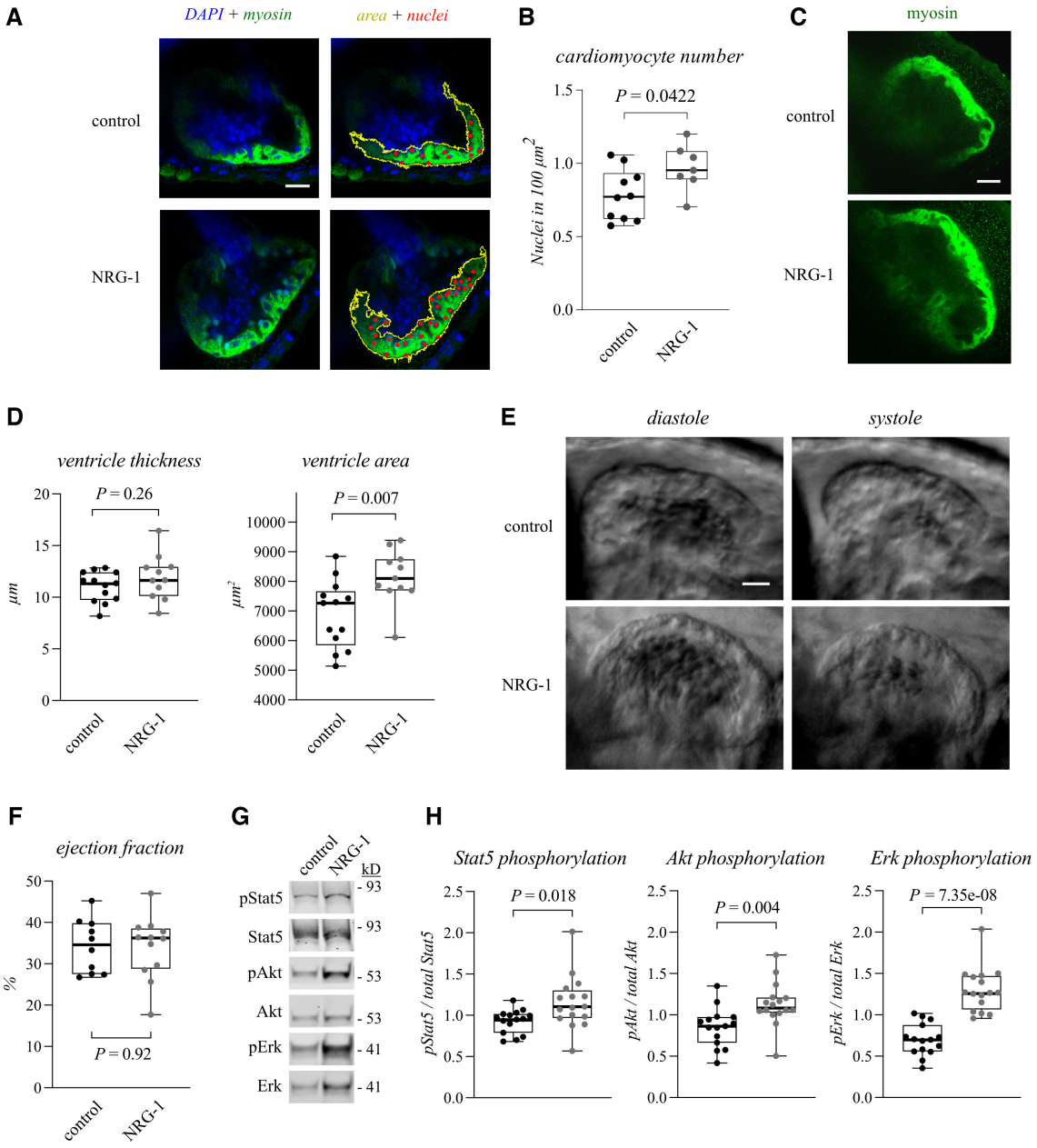

Figure 3. NRG-1 promotes hyperplastic myocardial growth and Stat5 activation in zebrafish embryos.

A–D Confocal images (A, C) and quantification (B, D) of immunofluorescence staining of myosin heavy chain (green) and DAPI (blue) in the hearts of 4 dpf zebrafish embryos injected with either the buffer control or NRG-1 into the pericardial sac at 2 dpf. The myosin immunoreactivity was used to quantify both the average thickness of the ventricular wall as well as the cross-sectional area of the ventricles. The number of nuclei was estimated with the DAPI stain. The number of nuclei (red) in the ventricle and the ventricle area (yellow) was quantified to differentiate between hypertrophic and hyperplastic growth. One dot in the boxplots corresponds to one heart (Control [A, B]: $n = 10$, NRG-1 [A, B]: $n = 7$, control [C, D]: $n = 13$, NRG-1 [C, D]: $n = 11$; biological replicates from two replicate experiments). Unpaired two-tailed *T*-test was used for statistics. Scale bars 20 µm.

E, F Still frame phase contrast images of *in vivo* imaging of the zebrafish embryo hearts (E) and quantification of ejection fractions (F). The zebrafish embryos were treated as in (A). The ejection fractions were calculated from the videos (Movies EV1 and EV2). One dot in the boxplot corresponds to the ejection fraction of one heart (Control: $n = 10$, NRG-1: $n = 12$; biological replicates from one of two replicate experiments). Unpaired two-tailed *T*-test was used for statistics. Scale bar 20 µm.

G, H Western analysis (G) and densitometric quantification (H) of Stat5, Akt and Erk phosphorylation in zebrafish embryos. The embryos were treated as in (A). One dot in the boxplots corresponds to the relative densitometric value of one pooled sample of 3–4 zebrafish embryos (Control: $n = 15$, NRG-1: $n = 16$; biological replicates combined from three replicate experiments). Unpaired two-tailed *T*-test with Welch's correction (Stat5) or unpaired two-tailed *T*-test (Erk, Akt) was used for statistics.

Data information: For all boxplots the central band represents the median, the box the interquartile range and whiskers the whole range of values.
Source data are available online for this figure.

with human STAT5b than with human STAT5a. These data indicate that in a zebrafish model of NRG-1-induced hyperplastic myocardial growth, Stat5 is activated by the Nrg-1/Erbb4 pathway.

Chemical inhibition of the Nrg-1/Erbb4 pathway results in reduced myocardial growth and Stat5 activation in zebrafish embryos

To assess the effect of the Nrg-1/Erbb4 pathway inhibition on the hyperplastic myocardial growth and Stat5 activation *in vivo*, zebrafish embryos were treated at 2 dpf for 2 days with DMSO or the ERBB inhibitors AG1478, lapatinib, or gefitinib. The function and the morphology of the ventricles was examined with live imaging (Fig 4A). The ERBB inhibitor AG1478 has been reported to inhibit ERBB1, ERBB2, and ERBB4 (Egeblad *et al*, 2001), lapatinib ERBB1 and ERBB2 (Xia *et al*, 2002), and gefitinib ERBB1 (Anderson *et al*, 2001). As expected, treatment with both inhibitors reported to inhibit the ERBB2/ERBB4 heterodimer in the myocardium significantly reduced the cross-sectional area of the ventricles, while treatment with the ERBB1 inhibitor gefitinib had no significant effect (Fig 4A and B). Treatment with AG1478 also reduced the thickness of the ventricular wall. The ejection fraction of all ERBB inhibitor-treated zebrafish, however, was retained although the AG1478- and lapatinib-treated ventricles displayed abnormal contractions (Movies EV3–EV6).

Consistent with the role of STAT5b downstream of ERBB4 activation in the mouse models (Fig 1C and D, H and I), treatment with the inhibitors targeting the ERBB2/ERBB4 heterodimer, but not the ERBB1 inhibitor, reduced Stat5 phosphorylation in zebrafish embryos (Fig 4C and D). Phosphorylation of Erk, however, was significantly reduced only by treatment with the ERBB1 inhibitor gefitinib. Signal for phospho-Akt, surprisingly, was induced by lapatinib and was not significantly affected by treatment with other ERBB inhibitors.

To examine the role of dynamin-2 in the hyperplastic growth and Stat5 activation, the embryos were treated at 2 dpf for 2 days with or without dynasore. The dynasore treatment resulted in both reduced ventricular area and ventricular wall thickness as compared to the control treatment (Fig 4E and F). The ejection fraction was, however, unaltered in the dynasore-treated ventricles indicating that the reduced myocardial growth did not lead to heart failure (Fig 4G and H, Movies EV7 and EV8).

Finally, the effect of dynasore on the activation of Stat5, Akt, and Erk signaling was analyzed (Fig 4I and J). Stat5 was significantly less active in the dynasore-treated zebrafish embryos as compared to the control, while no effect was observed for either Akt or Erk signaling. Taken together, the results indicate that the loss of myocardial growth due to inhibition of the Nrg-1/Erbb4/Dynamin-2 pathway correlates with the loss of Stat5, but not of Akt or Erk activation.

CRISPR/Cas9-mediated knockdown of the zebrafish stat5b gene results in reduced myocardial growth and heart failure in zebrafish embryos

To explore whether knockdown of the *stat5b* gene was sufficient to reduce myocardial growth, zebrafish embryos were injected with the recombinant CRISPR/Cas9 enzyme and control- or *stat5b*-targeting guide RNAs (gRNA) at one-cell stage. The efficacy of the *stat5b* knockdown was confirmed with genomic sequencing, real-time RT-PCR (Fig EV3A and B) and with immunofluorescence staining of whole-mount embryos (Fig 5A and B). The cross-sectional area of the ventricles of *stat5b* gRNA-injected 4 dpf embryos was significantly smaller when compared to the control gRNA-injected embryos (Fig 5A and B), indicating reduced myocardial growth.

The ejection fraction of the ventricles of *stat5b* gRNA-injected zebrafish embryos was also significantly reduced compared with the control gRNA-injected embryos (Fig 5C and D; Movies EV9 and EV10) suggesting heart failure. These results indicate that the down-regulation of Stat5b alone is sufficient to disrupt the normal growth and function of the myocardium.

Figure 4. Erbb4 pathway regulates myocardial growth and Stat5 activation in zebrafish embryos.

A, B Still frame phase contrast images of *in vivo* imaging of the zebrafish embryo hearts at 4 dpf (A) and quantification of heart dimensions and ejection fractions (B). The embryos were treated with the buffer control DMSO or the ERBB inhibitors AG1478, lapatinib or gefitinib for 2 days. The ventricular wall thickness, cross-sectional ventricular area, and ejection fraction was quantified from the videos (Movies EV3–EV6). One dot in the boxplots corresponds to one heart (DMSO: $n = 23$, AG1478: $n = 22$, Lapatinib: $n = 15$, Gefitinib: $n = 21$, for each group in ejection fraction panel: $n = 16$; biological replicates). One-way ANOVA and the Dunnett's multicomparison test with multiple test correction was used for statistics. Scale bar 50 μm.

C, D Western analysis (C) and densitometric quantification (D) of Stat5, Akt and Erk phosphorylation in zebrafish embryos. The embryos were treated as in (A). One dot in the boxplots corresponds to the relative densitometric value of one pooled sample of five zebrafish embryos (DMSO [Stat5] $n = 13$, AG1478 [Stat5] $n = 7$, Lapatinib [Stat5]: $n = 4$, Gefitinib [Stat5] $n = 6$, DMSO [Akt] $n = 9$, AG1478 [Akt] $n = 3$, Lapatinib [Akt] $n = 3$, Gefitinib [Akt] $n = 3$, DMSO [Erk] $n = 13$, AG1478 [Erk] $n = 6$, Lapatinib [Erk] $n = 4$, Gefitinib [Erk] $n = 8$; biological replicates combined from three replicate experiments). One-way ANOVA and the Dunnett's multicomparison test (Stat5, Akt) or non-parametric Kruskal-Wallis with Dunn's multicomparison test (Erk) was used for statistics.

E, F Confocal images (E) and quantification (F) of immunofluorescence staining of myosin heavy chain in hearts of 4 dpf zebrafish embryos treated with DMSO or dynasore for 2 days. The myosin immunoreactivity was used to quantify the average thickness of the ventricular wall and the cross-sectional area of the ventricles. One dot in the boxplots corresponds to one heart (DMSO [thickness, ejection fraction] $n = 11$, dynasore [thickness, ejection fraction] $n = 12$, DMSO [area] $n = 15$, dynasore [area] $n = 14$; biological replicates). Unpaired two-tailed *T*-test was used for statistics. Scale bar 50 μm.

G, H Still frame phase contrast images of *in vivo* imaging of the zebrafish embryo hearts (G) and quantification of ejection fractions (H). The zebrafish embryos were treated as in (E). The ejection fractions were calculated from the videos (Movies EV7 and EV8). One dot in the boxplot corresponds to the ejection fraction of one heart (DMSO: $n = 13$, dynasore: $n = 12$; biological replicates). Unpaired two-tailed *T*-test was used for statistics. Scale bar 50 μm.

I, J Western analysis (I) and densitometric quantification (J) of Stat5, Akt and Erk phosphorylation in zebrafish embryos. The embryos were treated as in (E). One dot in the boxplots corresponds to the relative densitometric value of one pooled sample of five zebrafish embryos (for each group $n = 5$; biological replicates). Unpaired two-tailed *T*-test was used for statistics.

Data information: For all boxplots the central band represents the median, the box the interquartile range and whiskers the whole range of values.
Source data are available online for this figure.

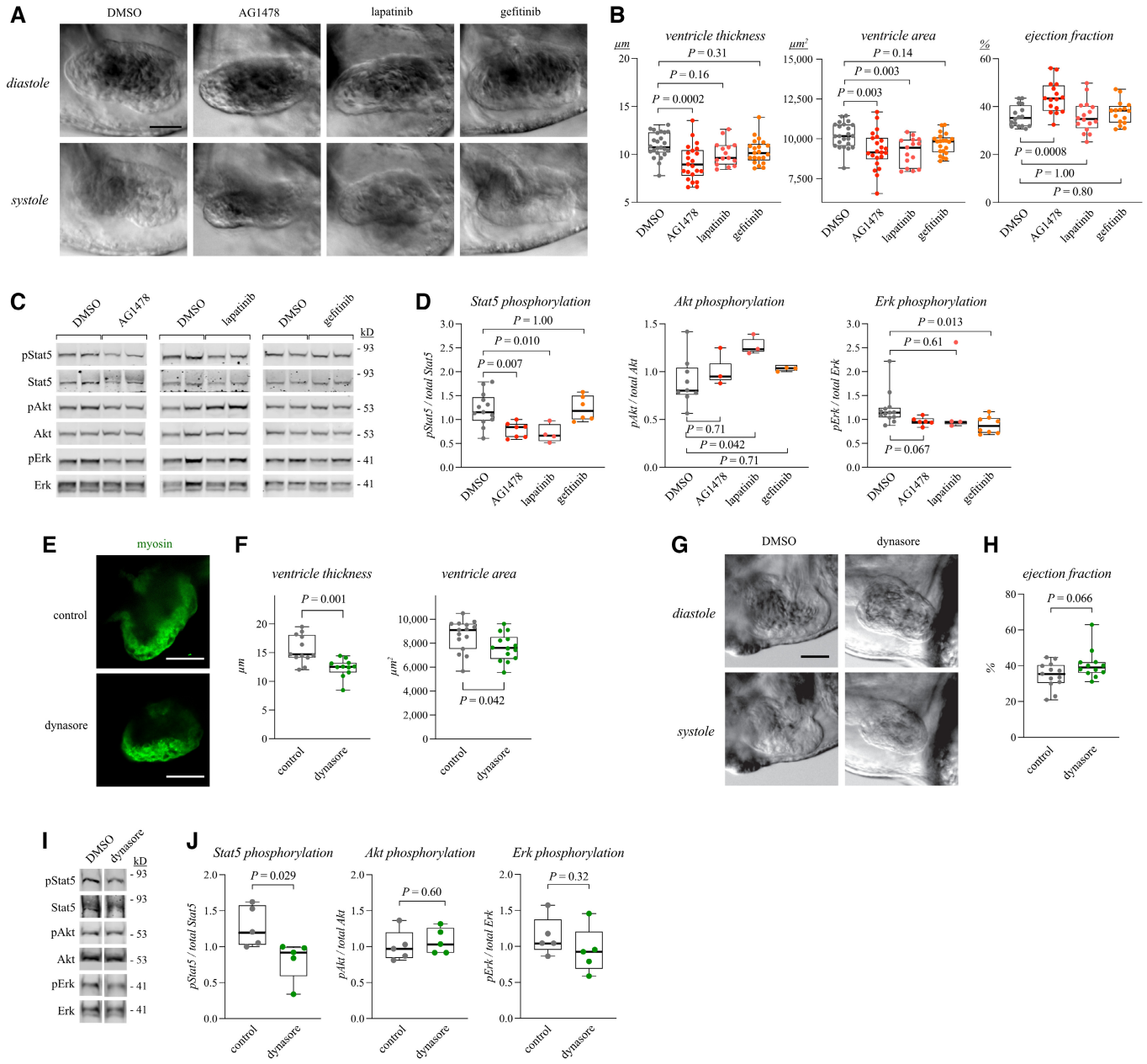

Figure 4.

Figure 5. *Stat5b* is necessary for cardiac growth and function in zebrafish embryos.

A, B Confocal images (A) and quantification (B) of immunofluorescence staining of myosin heavy chain and Stat5b in hearts of 4 dpf zebrafish embryos injected with CRISPR/Cas9 and either control or *stat5b*-targeting gRNA at one-cell stage. The myosin immunoreactivity was used to quantify the average thickness of the ventricular wall and the cross-sectional area of the ventricles. Stat5b staining intensity was also quantified. One dot in the boxplots corresponds to one heart (control gRNA: $n = 14$, *stat5b* gRNA $n = 13$; biological replicates from one of three replicate experiments). Unpaired two-tailed *T*-test was used for statistics. Scale bar 50 μm.

C, D Still frame phase contrast images of *in vivo* imaging of the zebrafish embryo hearts (C) and quantification of the ejection fraction (D). The 4 dpf embryos were treated as in A. Ejection fraction was quantified from the videos. One dot in the boxplots corresponds to ejection fraction of one heart (for each group $n = 22$; biological replicates from one of three replicate experiments). Unpaired two-tailed *T*-test was used for statistics. Scale bar 50 μm.

Data information: For all boxplots the central band represents the median, the box the interquartile range and whiskers the whole range of values.
Source data are available online for this figure.

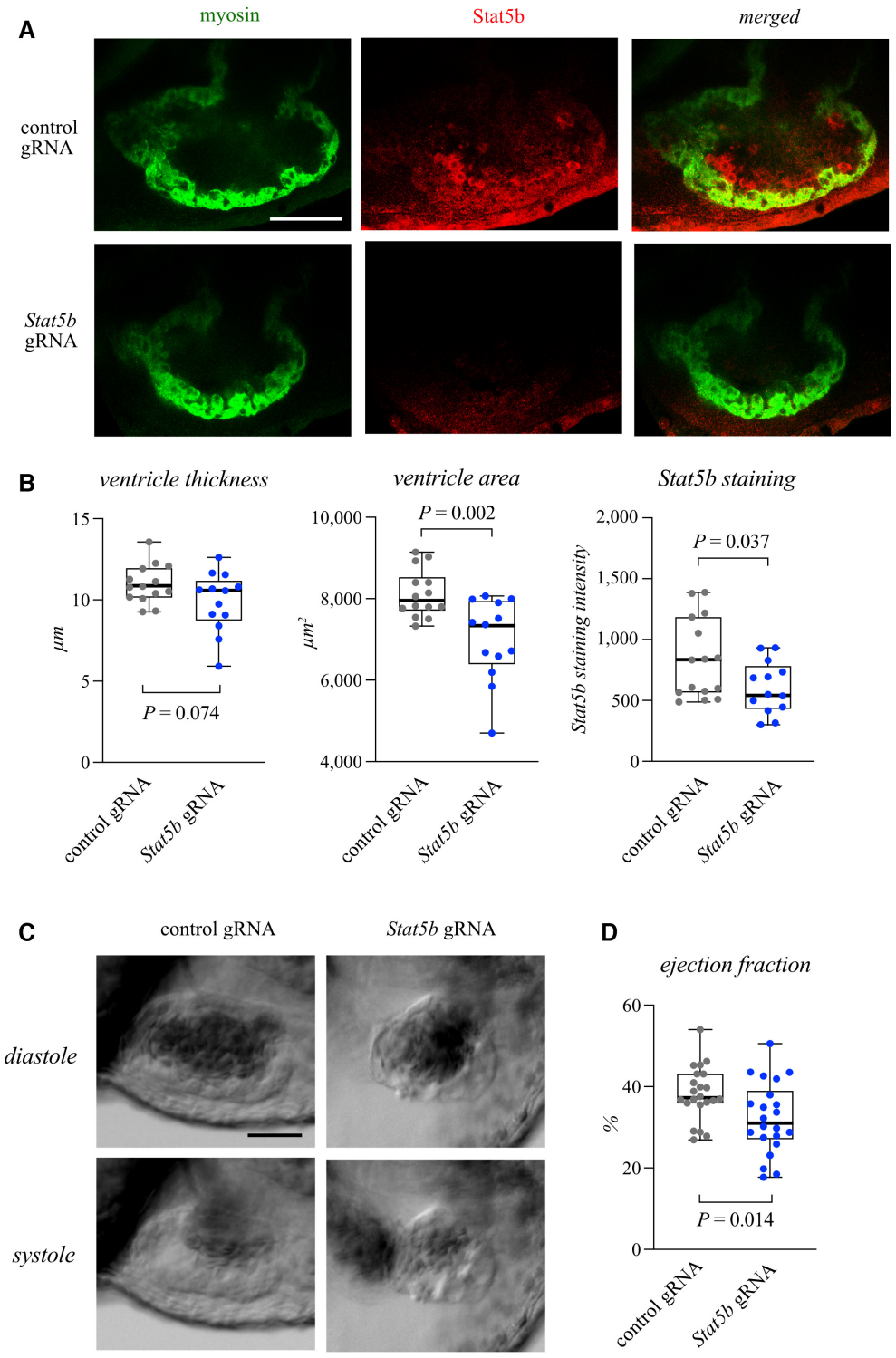

Figure 5.

The NRG-1/ERBB4/STAT5b signaling pathway is dysregulated in the myocardium of patients with pathological cardiac hypertrophy

Finally, to explore the role of the NRG-1/ERBB4/STAT5b signaling pathway in the context of pathological hypertrophic myocardial growth in human, the expression signature of the NRG-1/ERBB4/STAT5b signaling pathway and activation of STAT5b were investigated in clinical samples representing different types of pathological cardiac hypertrophy or normal heart tissue. First, pre-existing transcriptome datasets were subjected to principal component analysis to observe whether control subjects and patients suffering from

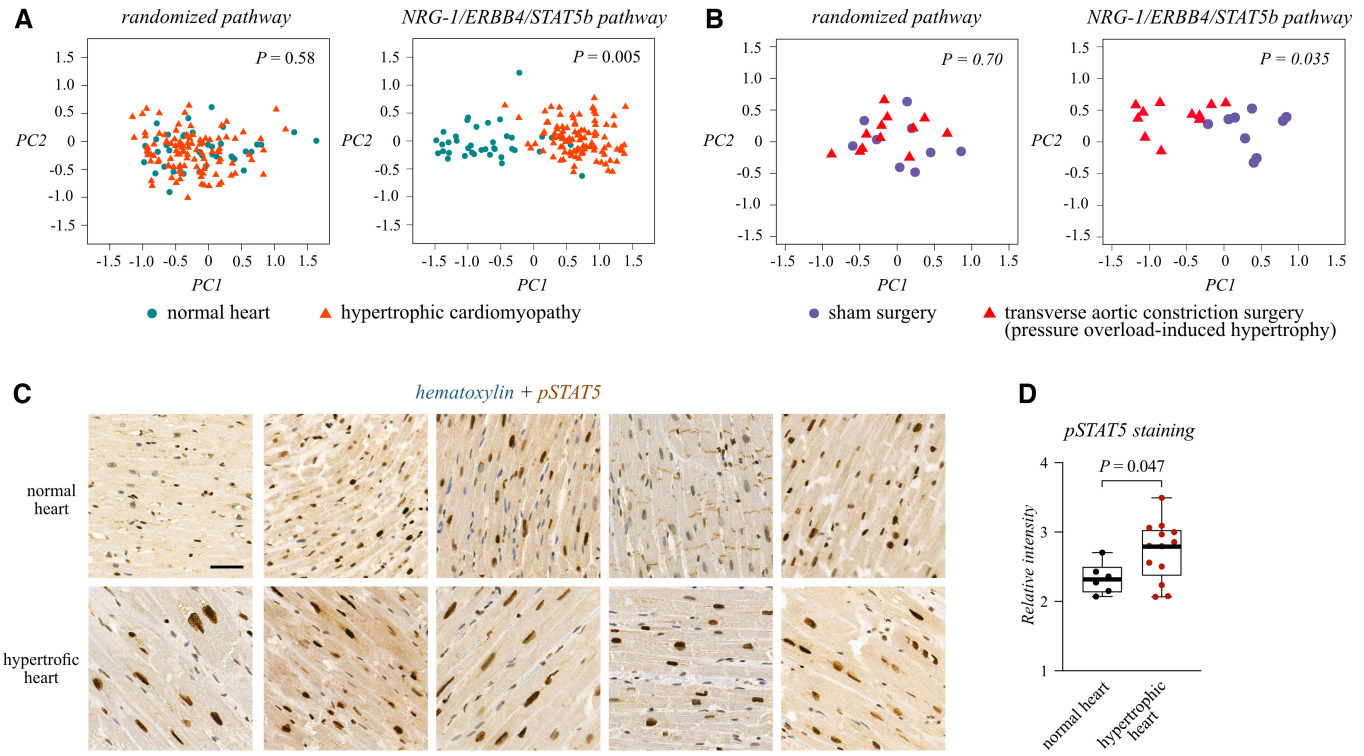

Figure 6. NRG-1/ERBB4/STAT5b signaling pathway is perturbed in pathological cardiac hypertrophy.

A Principal component and cluster analysis of transcripts of the NRG-1/ERBB4/STAT5b pathway (including the genes: *NRG1*, *ERBB4*, *STAT5B*, *IGF1*, *MYC* and *DNM2*) with clinical samples representing normal myocardium or hypertrophic cardiomyopathy. The dataset GSE36961 was acquired from the Gene Expression Omnibus database (Data ref: Hebl *et al*, 2012). One symbol in the plots corresponds to one subject (normal: $n = 39$, hypertophic cardiomyopathy $n = 106$; biological replicates). Statistical significance of clusterization was calculated by estimating a probability distribution for the relative distance within a cluster and between clusters and by drawing the cumulative probability from the resulting empirical cumulative probability function.

B Principal component and cluster analysis of transcripts of the NRG-1/ERBB4/STAT5b pathway with samples representing myocardia of mice subjected to sham or transverse aortic constriction surgery. The dataset GSE5500 was acquired from the Gene Expression Omnibus database (Data ref: Bisping *et al*, 2006). One symbol in the scatterplots corresponds to one mouse (sham: $n = 9$, transverse aortic constriction: $n = 12$; biological replicates).

C, D Immunohistochemical analysis (C) and quantification (D) of STAT5 activation in sections representing normal myocardia or pathological cardiac hypertrophy ($n = 3$, aortic stenosis; $n = 2$, idiopathic cardiomyopathy). Phospho-STAT5b staining intensity was quantified. One dot in the boxplot corresponds to one subject (normal: $n = 6$, hypertrophic $n = 13$; biological replicates). In the boxplot the central band represents the median, the box the interquartile range and whiskers the whole range of values. Unpaired two-tailed *T*-test was used for statistics. Scale bar 50 μm.

Source data are available online for this figure.

hypertrophic cardiomyopathy could be segregated based on the expression levels of the genes in the NRG-1/ERBB4/STAT5b signaling pathway (Figs 6A and EV4A). The details of the datasets can be accessed through the Gene Expression Omnibus database (Edgar *et al*, 2002; Barrett *et al*, 2013) with the GSE prefix identifiers indicated in the figure legends of Fig 6 and in the Fig EV5. The dimensionality reduction of the expression level of the NRG-1/ERBB4/STAT5b signaling pathway genes indeed was able to significantly cluster cases with pathological cardiac hypertrophy and those without into separate groups in three independent datasets. The successful segregation indicates that the NRG-1/ERBB4/STAT5b signaling pathway genes are consistently differentially regulated in hypertrophic vs. normal cardiac tissue. The transcripts of *MYC*, *IGF1* and *NRG1* genes were most differentially regulated in the NRG-1/ERBB4/STAT5b signaling pathway, as indicated by the principal component weights (Fig EV4B).

The role of NRG-1/ERBB4/STAT5b signaling pathway in pressure overload-induced pathological cardiac hypertrophy was also investigated from datasets representing cardiac transcriptomes of mice that had undergone transverse aortic constriction surgery (TAC) or sham surgery. The dimensionality reduction in the expression level of the NRG-1/ERBB4/STAT5b signaling pathway genes led to a statistically significant clustering of the TAC- and sham-treated mice into separate groups in three independent datasets (Figs 6B and EV4C). The successful segregation indicates that NRG-1/ERBB4/STAT5b signaling pathway genes are also differentially regulated in pressure overload-induced cardiac hypertrophy. The principal component weights suggested that *Igf1* and *Dnm2* were most differentially regulated by the TAC vs. sham surgery (Fig EV4D).

The activation of STAT5b in control subjects and patients suffering from pathological cardiac hypertrophy due to aortic stenosis, alcoholic cardiomyopathy, or idiopathic cardiomyopathy was investigated with immunohistochemistry. Formalin-fixed paraffin-embedded (FFPE) sections from cardiac left ventricle were acquired from the Auria Biobank (University Hospital of Turku, Finland).

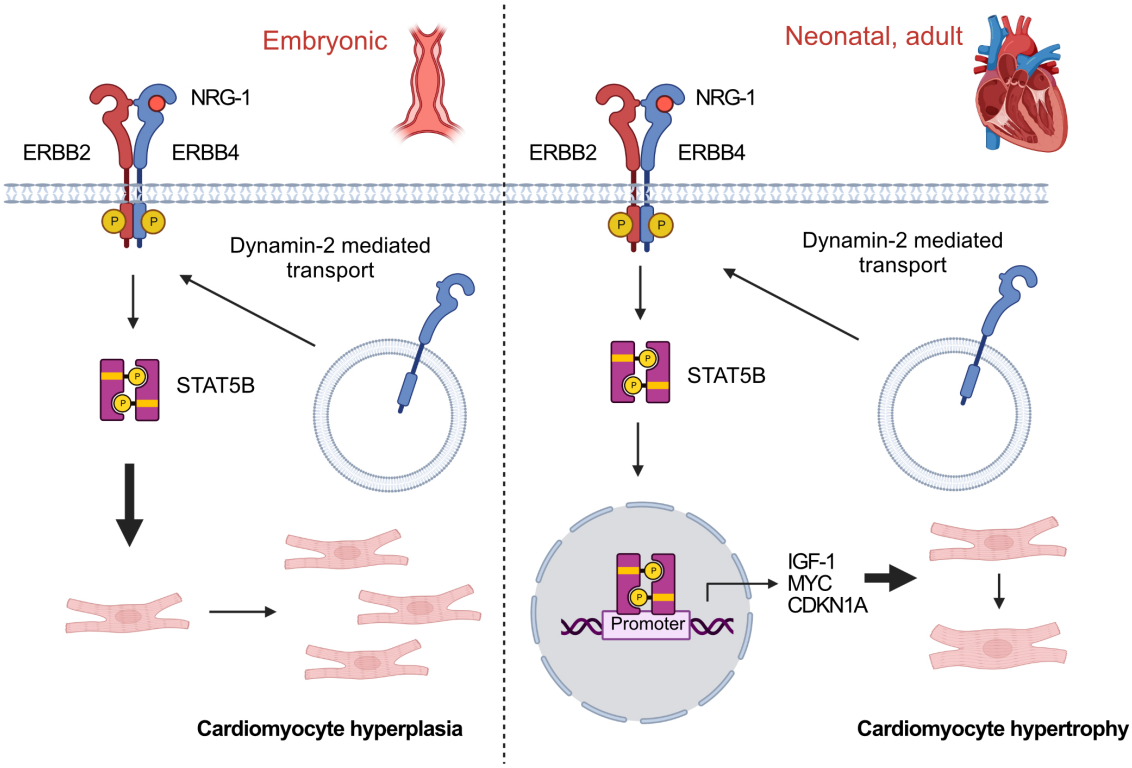

Figure 7. The proposed NRG-1/ERBB4/STAT5b pathway in cardiac growth.
The pathway may regulate both cardiomyocyte hyperplasia (left) and hypertrophy (right) at different developmental stages.

Both heart weight and cardiomyocyte size were greater in the samples representing pathological cardiac hypertrophy (Fig EV4E). The heart sections were stained with an antibody that recognizes the phosphorylated state of the activating residue of STAT5b, and the immunosignal was quantified from cardiomyocytes in representative randomly selected regions. The specificity of the immunosignal was controlled in FFPE samples treated with insulin or control or STAT5 targeting siRNAs (Fig EV5A–D). The signal of the phosphorylated STAT5 in cardiomyocyte nuclei was significantly greater in the cases representing pathological cardiac hypertrophy as compared to the controls (Fig 6C and D; only five cases from both cohorts visualized) indicating that STAT5b activation is upregulated in pathologically hypertrophic myocardium in human. Taken together, these results suggest that the NRG-1/ERBB4/STAT5b pathway is dysregulated in mammalian pathological cardiac hypertrophy.

Discussion

A recent review identified the effect of NRG-1 on cardiomyocyte growth as one of the translationally relevant but poorly understood aspects of cardiovascular research, and called for further research on the underlying molecular mechanisms (De Keulenaer *et al*, 2019). Here, we focused on the signaling pathway of NRG-1 in primary cardiomyocytes and in the heart tissue of mouse and embryonic zebrafish to elucidate the molecular mechanisms of NRG-1-mediated cardiomyocyte growth. The NRG-1 receptor ERBB4, the ERBB4-activated signal transducer STAT5b, and dynamin-2, which was discovered to control the subcellular localization of ErbB4, were identified as key effectors controlling both hyperplastic cardiomyocyte growth during embryogenesis as well as hypertrophic cardiomyocyte growth at neonatal and adult stages (Fig 7). The expression of two transcription factors known as essential regulators of cardiac growth, IGF-1 and MYC, was controlled by NRG1/ERBB4/STAT5b signaling in neonatal and adult cardiomyocytes. We also found evidence of activation of the NRG1/ERBB4/STAT5b signaling in human samples displaying increased myocardial growth.

In this study, the role of STAT5b in NRG-1-induced cardiomyocyte growth was examined across species. While cardiac NRG-1 signaling has mostly been analyzed in mouse models, the reports of zebrafish embryos have produced similar findings. In both species, the genetic or chemical disruption of genes along the NRG-1/ERBB pathway leads to the loss of cardiac trabeculation and attenuated growth of the ventricular wall (Gassmann *et al*, 1995; Lee *et al*, 1995; Meyer & Birchmeier, 1995; Liu *et al*, 2010; Rasouli & Stainier, 2017). Few reports have suggested that in zebrafish embryos, cardiac trabeculation is not dependent on the Nrg-1 ligand, but on another Erbb4 ligand, Nrg-2a, which has similar expression pattern in endothelial cells as NRG-1 in mice (Samsa *et al*, 2016; Rasouli & Stainier, 2017). Overexpression of the zebrafish *nrg1* gene, however, has induced cardiomyocyte proliferation in adult zebrafish (Gemberling *et al*, 2015). Similarly, our findings indicated that the administration of human recombinant NRG-1 did

induce hyperplastic cardiomyocyte growth in zebrafish embryos. It is of note that the molecular mechanisms regulating cardiac function and growth in mice and zebrafish are expected to be different in adulthood when zebrafish cardiomyocytes retain their regenerative capability through cardiomyocyte hyperplasia in much larger quantities than in adult mice (Poss *et al*, 2002).

The ERK pathway has been established as one of the main pathways regulating hypertrophic cardiomyocyte growth downstream of several stimuli (Gallo *et al*, 2019). The NRG-1/ERBB pathway promotes ERK1/2 phosphorylation in cardiomyocytes; therefore, NRG-1-induced cardiomyocyte hypertrophy has been attributed to ERK signaling (Baliga *et al*, 1999; Fukazawa *et al*, 2003; Kuramochi *et al*, 2006). A recent report, however, suggests that the activation of ERK signaling alone is not sufficient to confer NRG-1-mediated cardiomyocyte hypertrophy (Wang *et al*, 2021). This is consistent with several reports where treatment with an anti-ERBB2 antibody or *ERBB2*-targeting siRNAs has been unable to reduce the phosphorylation of ERK1/2 in cardiomyocytes (Sawyer *et al*, 2002; Kuramochi *et al*, 2006; Wang *et al*, 2021). Treatment with *ERBB4* shRNA has drastically reduced hypertrophic growth but similarly has only led to a slight reduction of ERK1/2 phosphorylation in cardiomyocytes (Wang *et al*, 2021). The conditional double knockout of *Erk1/Erk2* in mice leads to dilated cardiomyopathy resembling the loss of the genes along the NRG-1/ERBB2/ERBB4 pathway (Kehat *et al*, 2011). The histology of the dilated ventricles, however, is markedly different between the conditional double *Erk1/Erk2* knockout model and the conditional *Nrg1/Erbb2/Erbb4* pathway knockout models. The cardiomyocytes in the double *Erk1/Erk2* knockout model are elongated and show a loss of concentric hypertrophic response (Kehat *et al*, 2011), while the cardiomyocytes in the *Erbb2/Erbb4* knock-out models are hypertrophic (Özcelik *et al*, 2002; García-Rivello *et al*, 2005). The asymmetry in the cardiomyocyte morphology of the *Erk1/Erk2* vs *Erbb2/Erbb4* conditional knockout model hearts and the lack of response in ERK phosphorylation after downregulation of ERBB2 or ERBB4 are consistent with our observations here of NRG-1/ERBB4 additionally activating STAT5b in murine *in vitro* and *in vivo* models of hypertrophic growth. Indeed, the NRG-1/ERBB4-mediated hypertrophic cardiomyocyte growth was reduced by STAT5b knock-down.

The NRG-1-mediated hyperplastic growth in turn has been attributed to PI3K/AKT signaling in adult cardiomyocytes based on an experiment, in which the expression of PTEN, the negative regulator of PI3K signaling, reduced DNA synthesis (Bersell *et al*, 2009). According to the results presented here, the activation of Stat5b was consistently modulated by intervention of the Nrg-1/Erbb4 signaling pathway, while the phosphorylation of Erk and Akt was significantly modulated by NRG-1 injections but not by chemical inhibition of the Nrg-1/Erbb4 pathway in embryonic zebrafish models of hyperplastic myocardium growth. These observations suggest that proliferation of cardiomyocytes is STAT5b dependent during embryogenesis. Whether STAT5b contributes to the proliferation of adult cardiomyocytes remains to be addressed.

The NRG-1/ERBB pathway is not the only pathway that has been associated with myocardial growth. Several other pathways have been identified as essential for cardiomyocyte proliferation, hypertrophy, and dedifferentiation, which allows for adult cardiomyocytes to re-enter the cell cycle. These pathways have been extensively reviewed in previous reports and include, the FGF-1, IGF-1, Ang-II, Hippo, and Wnt signaling cascades (Nakamura & Sadoshima, 2018; Bongiovanni *et al*, 2021). The role of several miRNAs and transcription factors similarly have been established in controlling the expression of genes with central roles in regulating cell cycle and growth of cardiomyocytes (Lock *et al*, 2018; Bongiovanni *et al*, 2021). As of yet it is, however, unclear which of these signals are the master regulators of cardiomyocyte growth. In a previous report, the ErbB2-mediated activation of STAT5 was sufficient to override the Hippo pathway-induced withdrawal from cell cycle (Hirai *et al*, 2017), and our findings indicate that the expression of IGF-1 in neonatal and adult cardiomyocytes is dependent on NRG-1, ERBB4 and STAT5b. Thus, it is plausible that the NRG-1/ERBB4/STAT5b pathway is an upstream regulator of the IGF-1 and Hippo pathways in the myocardium. Any further role of the NRG-1/ERBB4-activated STAT5b in the interplay of all these growth and cell cycle signals that converge to induce myocardial growth remains to be elucidated.

Similar to NRG-1 and ERBB4 (De Keulenaer *et al*, 2019), STAT5b has previously been proposed to have role in the molecular pathogenesis of heart failure. Indeed, a polymorphism in the exon 1 of the *STAT5B* gene has been associated with the risk for dilated cardiomyopathy (Peng *et al*, 2012). Here, we identified differential regulation of the NRG-1/ERBB4/DNM2/STAT5b signaling in clinical samples of pathological cardiac hypertrophy independent of the etiology. This is consistent with previous observations that chemical inhibition of STAT5 reduces pathological cardiac hypertrophy in *in vivo* mouse models (Kimura *et al*, 2018; Jin *et al*, 2022). Pathological cardiac hypertrophy is a compensatory response that can precede heart failure and ERBB4 expression has been reported to be downregulated in cases in which cardiac hypertrophy has advanced to heart failure (Rohrbach *et al*, 1999, 2005b). In our zebrafish model, the CRISPR/Cas9-mediated knockdown of *stat5b* also led to reduced ejection fraction indicative of heart failure. Further experimentation is, however, needed to understand the role of STAT5b in pathological cardiac hypertrophy and its progression to heart failure.

STAT5b has been suggested to mediate the cardioprotective effect of remote ischemic preconditioning in a murine model of ischemic cardiac injury and in clinical samples (Heusch *et al*, 2012; Wu *et al*, 2017; Chen *et al*, 2018). The results presented here further support the therapeutic potential of STAT5b by introducing STAT5b as one of the downstream effectors of NRG-1 in the heart. NRG-1 signaling has been found to attenuate cardiac injury in several animal models including, for example, ischemia, doxorubicin, metabolic stress, and pacing-induced cardiac injury models (Odiete *et al*, 2012; Mendes-Ferreira *et al*, 2013). The cardioprotective effect of NRG-1 has been attributed to increased PI3K/AKT signaling (Odiete *et al*, 2012; Mendes-Ferreira *et al*, 2013). Interestingly in the murine model of ischemic cardiac injury and remote ischemic preconditioning the cardioprotective PI3K/AKT signaling was activated downstream of STAT5b (Chen *et al*, 2018). Consistently, chemical inhibition of STAT5 has been shown to downregulate PI3K/AKT signaling in a mouse model of pressure overload induced cardiac hypertrophy (Kimura *et al*, 2018). Together these observations putatively suggest that the NRG-1-induced cardioprotective PI3K/AKT signaling is dependent on STAT5b. Whether the cardioprotective effect of NRG-1 truly is dependent on STAT5b and whether, for example, targeting the deactivating phosphatases of STAT5b (Yu *et al*, 2000; Rigacci *et al*, 2008; Huang *et al*, 2012) or

repressors of STAT5b-induced transcription (Nakajima *et al*, 2001; Sefat-E-Khuda *et al*, 2004; Martens *et al*, 2005) in the myocardium could serve as an approach with therapeutic potential in heart failure remains to be formally addressed. In accordance with clinical applicability, administration of NRG-1 and the protein product of the STAT5b target gene *IGF1* has demonstrated success in attenuating dilated cardiomyopathy in clinical trials (Welch *et al*, 2002; Liu *et al*, 2006; Komamura, 2017).

In addition to STAT5b, the membrane-remodeling GTPase dynamin-2 was identified as a regulator of NRG-1/ERBB4 signaling promoting cardiomyocyte growth. Inhibition of dynamin GTPase activity reduced ERBB4 at the cell surface as well as STAT5b activation and NRG-1-induced cardiomyocyte and myocardial growth in zebrafish embryos. Expression of dynamin-2 has previously been reported to be decreased in heart failure in isopretenol-induced rat heart failure model and in clinical samples (Li *et al*, 2013). It has also been demonstrated that decreased dynamin-2 expression leads to cardiomyocyte apoptosis by stimulating Ca^{2+} influx from the sarcolemma (Li *et al*, 2013). Interestingly, several reports also indicate a role for NRG-1/ERBB4 signaling in regulating cardiomyocyte apoptosis (Rohrbach *et al*, 2005a; Jie *et al*, 2012; Cohen *et al*, 2014), suggesting that cardiomyocyte apoptosis induced by dynamin-2 deficiency (Li *et al*, 2013) could be mediated by the loss of NRG-1/ERBB4 signaling. Consistently, STAT5b has been shown to regulate the expression of the anti-apoptotic Bcl2 and Bcl2-XL in the myocardium (Chen *et al*, 2018). During induced cardiac hypertrophy, no significant level of apoptosis has been detected in the myocardium (Romano & Ceci, 2020), which is consistent with the observations here of elevated STAT5b activation in states of increased hypertrophic myocardial growth.

Materials and Methods

The details of the reagents, experimental models, instruments, and tools used are provided in the Reagents and Tools table. The sequences for the oligonucleotides utilized in this study are provided in Table EV1.

Reagents and Tools table

Reagent/resource	Reference or source	Identifier or catalog number
Experimental models		
HEK293T cell line	ATCC	CRL-3216
MDA-MB-468 pBABE Puro ErbB4 JM-a cell line	Described earlier (Sundvall *et al*, 2012)	
MDA-MB-468 pBABE Puro ErbB4 JM-b cell line	Described earlier (Sundvall *et al*, 2012)	
MDA-MB-468 pBABE Puro empty vector cell line	Described earlier (Sundvall *et al*, 2012)	
MCF-7 cell line	ECACC	86012803
HC11 cell line	ATCC	CRL-3062
C57BL/6JOlaHsd (*Mus musculus*)	Envigo Harlan	C57BL/6JOlaHsd
Primary cultures from 1 to 3 days old male wildtype NMRI (*Mus musculus*)	Janvier labs	RjHan:NMRI
Casper strain (roy, mitfa) (*Danio rerio*)	Described earlier (White *et al*, 2008)	
Patient samples	Auria Biobank	
Recombinant DNA		
pMD2.G (env)	Addgene	12259
pMDLg/pRRE (gag, pol, RRE)	Addgene	12251
pRSV-Rev (Rev)	Addgene	12253
pc DNA 3.1 ERBB4 JM-a CYT-2 –HA Hyg(+)	Described earlier (Maatta *et al*, 2005)	
pc DNA 3.1 ERBB4 JM-b CYT-2 –HA Hyg(+)	Described earlier (Maatta *et al*, 2005)	
pc DNA 3.1 Hyg(+)	Described earlier (Maatta *et al*, 2005)	
Control shRNA: sh-scramble plasmid	Addgene	1864
Antibodies		
Mouse monoclonal anti-β-actin (AC-74), 1:10,000 (W)	Sigma	A5441
Mouse monoclonal anti-Akt (pan) (40D4), 1:1,000 (W)	Cell Signaling	2020S
Rabbit polyclonal anti-Phospho-Akt (Ser473) (D9E) XP®, 1:1,000 (W)	Cell Signaling	4060
Goat polyclonal anti-Dynamin II (C-18), 1:1,000 (W), 1:100 (PLA)	Santa Cruz	sc-6400
Rabbit monoclonal anti-ERBB4 (E200), 1:1,000 (W), 1:100 (PLA), 1 µg/1 mg protein (IP)	Abcam	ab32375

Reagents and Tools table (continued)

Reagent/resource	Reference or source	Identifier or catalog number
Mouse monoclonal anti-ERBB4 (HFR-1), 1:50 (IF), 1:100 (PLA), 1 µg/1 mg protein (IP)	Abcam	ab19391
Rabbit monoclonal p44/42 MAPK (Erk1/2), 1:1,000 (W)	Cell Signaling	9102
Rabbit polyclonal P-p44/42 MAPK (T202/Y204), 1:1,000 (W)	Cell Signaling	9101
Mouse monoclonal anti-myosin heavy chain (MF-20), 1:1,000 (W), 1:50–200 (IF)	DSHB	MF 20
Rabbit polyclonal anti-STAT5b, 1:500 (W), 1:20 (IF)	R&D	AF1584
Rabbit polyclonal anti-STAT5b, 1:500 (W), 1:50 (IF)	Sigma	SAB2102320
Rabbit polyclonal anti-Phospho-STAT5 (Tyr694), 1:500 (W)	Cell Signaling	9351
Recombinant Rabbit Anti-STAT5 (phospho Y694) antibody [E208], 1:1,000 (IHC)	Abcam	ab32364
Mouse monoclonal TPM1 antibody, mouse tropomyosin, striated muscle (CH-1)	DSHB	CH-1
Rabbit anti-goat IgG-HRP, 1:10,000 (W)	Santa Cruz	sc-2768
Goat anti-mouse IgG-HRP, 1:10,000 (W)	Santa Cruz	sc-2005
Goat anti-rabbit IgG-HRP, 1:10,000 (W)	Santa Cruz	sc-2004
IRDye® 680RD Donkey anti-Mouse IgG (H + L), 1:15,000 (W)	LI-COR	925-68072
IRDye® 800CW Donkey anti-Mouse IgG (H + L), 1:15,000 (W)	LI-COR	925-32212
IRDye® 680RD Donkey anti-Rabbit IgG (H + L), 1:15,000 (W)	LI-COR	926-68073
IRDye® 800CW Donkey anti-Rabbit IgG (H + L), 1:15,000 (W)	LI-COR	925-32213
Goat anti-Mouse IgG (H+L) Highly Cross-Adsorbed Secondary Antibody, Alexa Fluor 488, 1:100–500 (IF)	Invitrogen	A-11029
Goat anti-Rabbit IgG (H+L) Highly Cross-Adsorbed Secondary Antibody, Alexa Fluor 555	Invitrogen	A-21429
Oligonucleotides and other sequence-based reagents		
PCR primers	This study	Table EV1
Universal probe #21 (Cdkn1a)	Roche	4686942001
Universal probe #34 (Igf1)	Roche	4687671001
Universal probe #77 (Myc)	Roche	4689003001
Universal probe #77 (Stat5b)	Roche	4689003001
Universal probe #66 (Tpt1)	Roche	4688651001
The Universal Probe Library Mouse GAPDH Gene Assay	Sigma	5046211001
Prime Time Std qPCR Assay, B2m	IDT	Mm.PT.39a.22214835
Prime Time Std qPCR Assay, Ppia	IDT	Mm.PT.39a.2.gs
Universal probe #147 (rlp13a)	Roche	4694333001
siRNA control: AllStars Negative Control siRNA	Qiagen	SI03650318
siRNA DNM2#1: Silencer® Select DNM2 siRNA	Thermo Fisher Scientific	s4212
siRNA DNM2#2: Silencer® Select DNM2 siRNA	Thermo Fisher Scientific	s4213
Hs_STAT5A_2 FlexiTube siRNA	Qiagen	SI00048426
Hs_STAT5B_3 FlexiTube siRNA	Qiagen	SI00100408
shRNAs	This study	Table EV1
Alt-R® CRISPR-Cas9 Negative Control crRNA #1	IDT	1072544
crRNAs	This study	Table EV1
Alt-R® CRISPR-Cas9 tracrRNA	IDT	1072532
Chemicals, enzymes and other reagents		
Tyrphostin AG-1478	Cayman Chemicals	10010244
	Immunologic	DPVB55HRP

Reagents and Tools table (continued)

Reagent/resource	Reference or source	Identifier or catalog number
BrightVision Goat Anti- Mouse/Rabbit IgG HRP two step detection system		
BrightDiluent, normal antibody diluent	Immunologic	Bd09-125
BS3 (bis(sulfosuccinimidyl)suberate)	Thermo Fisher Scientific	21580
Cardiomyocyte Isolation Enzyme 1 (with papain)	Thermo Fisher Scientific	88288
Cardiomyocyte Isolation Enzyme 2 (with thermolysin)	Thermo Fisher Scientific	88289
Carnitine	Santa Cruz	sc-205727A
Creatine	Santa Cruz	sc-214774A
DAPI (4′,6-diamidino-2-phenylindole)	Sigma	D9542
DMEM	Lonza	12-614F
DMSO, Dimethyl Sulfoxide, Fisher BioReagents™	Thermo Fisher Scientific	BP231-100
DSP (dithiobis(succinimidyl propionate)), Lomant's Reagent	Thermo Fisher Scientific	22585
DTBP (Wang and Richard's Reagent)	Thermo Fisher Scientific	20665
Dynasore	Calbiochem	324410
Duolink® In Situ PLA® Probe Anti-Rabbit PLUS Affinity purified Donkey anti-Rabbit IgG (H + L)	Sigma	DUO92002
Duolink® In Situ PLA® Probe Anti-Goat MINUS Affinity purified Donkey anti-Goat IgG (H + L)	Sigma	DUO92006
Duolink® In Situ Detection Reagents Orange	Sigma	DUO92007
Estrogen	Sigma	E2758
Fugene 6	Promega	E2691
PureProteome™ Protein G Magnetic Bead System	Millipore	LSKMAGG10
Protein G-sepharose™ 4 Fast Flow	GE Healthcare	17-0618-01
EGF human, recombinant	Sigma	E9644
Fetal bovine serum	Biowest	S1810-500
Gefitinib	Cayman Chemicals	13166
Gelatin	Sigma	G-1890
HBSS	Thermo Fisher Scientific	88284
Hilymax	Dojindo	H357
Horse serum	GIBCO	16050-122
Mayer's hematoxylin	Sigma	03971
Matrigel® Growth Factor Reduced	Corning	356231
Medium 199	Sigma	M2520
EnGen Cas9 NLS	New England Biolabs	M0646T
Lapatinib	Selleckchem	S2111
Laemmli SDS sample buffer, reducing (6×)	Alfa aesar	J61337
Lipofectamine 2000	Thermo Fisher Scientific	11668019
Pronase E	Serva	33635.02
Recombinant Human NRG-1-beta 1	R&D	396-HB
Matrigel (growth factor reduced)	Corning	356231
Mowiol® 4-88	Sigma	475904
Nuclease-free duplex buffer	IDT	11-01-03-01
Penicillin-Streptomycin Mixture	Lonza	DE17-603E
Percoll Plus	GE Healthcare	17-5445-02
Pertex® Mounting Medium	Histolab	00811-EX
Phenol red solution	Sigma	P0290

Reagents and Tools table (continued)

Reagent/resource	Reference or source	Identifier or catalog number
Protease inhibitor cocktail	Thermo Fisher Scientific	A32957
ReproSil-Pur 5 µm 200 Å C18-AQ beads	Dr. Maisch	r15.aq.
RPMI 1640	Lonza	BE04-558F
SensiFAST cDNA Synthesis Kit	Bioline	BIO-65054
TaqMan universal Master Mix II	Applied Biosystems	4440038
Taq I polymerase	Thermo Fisher Scientific	P0401
Taurine	Santa Cruz	sc-202354
tC18 SepPak 96-well plate	Waters	86002321
Tricaine methane-sulfonate	Finquel, Argent Laboratories	MS-222
NucleoSpin TriPrep	Macherey-Nagel	740966.50
Trisure	Bioline	BIO-38033
Tris-EDTA pH 9,0	Biosite	BSC-20B1M
Trypsin/EDTA	Lonza	CC-5012
Trypsin Protease, MS Grade	Thermo Fisher Scientific	90057
UltraGlutamine	Lonza	BE17-605E/U1
Software		
GraphPad Prism 8.4.2	GraphPad Software (https://www.graphpad.com/)	
Matlab 2016a	MathWorks (https://mathworks.com/products/matlab.html)	
FiJi v1.53c	Described earlier (Schindelin *et al*, 2012; https://imagej.net/software/fiji/)	
Image Studio Lite v5.2	Li-COR (https://www.licor.com/bio/image-studio-lite/)	
CaseViewer v2.3	3DHISTECH (https://www.3dhistech.com/solutions/caseviewer/)	
QuantStudio 12K Software v1.4	Thermo Fisher Scientific	
MaxQuant v1.3	Described earlier (Cox & Mann, 2008)	
Metamorpheus (version 0.0.312)	Described earlier (Solntsev *et al*, 2018)	
FlashLFQ	Described earlier (Millikin *et al*, 2018)	
SpatTrack v2	Described earlier (Lund *et al*, 2014)	
colocalization algorithm of Villalta et al	Described earlier (Villalta *et al*, 2011)	
R v3.6.1	R Core Team (R Core Team, 2017; https://www.r-project.org/)	
RStudio v1.2.1335	RStudio team (RStudio team, 2019; https://www.posit.co)	
BioRender	https://www.biorender.com	
Other		
TC20 Automated Cell Counter	Bio-Rad	1450102
Motorized pellet pestle	Sigma	Z359971
Zeiss LSM 780 confocal microscope	Zeiss (https://www.zeiss.com/microscopy/en/home.html)	
Zeiss LSM 880 confocal microscope	Zeiss (https://www.zeiss.com/microscopy/en/home.html)	
Zeiss AxioZOOM.V16	Zeiss (https://www.zeiss.com/microscopy/en/home.html)	
Labvision autostainer	Thermo Fisher Scientific	A80500024
Pannoramic P1000 slide scanner	3DHISTECH	

Reagents and Tools table (continued)

Reagent/resource	Reference or source	Identifier or catalog number
QuantStudio 12K Flex Real-Time PCR System	Thermo Fisher Scientific	
Odyssey DLx	Li-COR	
Nanoject II microinjector	Drummond Scientific	
Nanodrop spectrophotometer	Thermo Fisher Scientific	
Thermo Fisher Scientific LTQ Orbitrap XL mass-spectrometer	Thermo Fisher Scientific	
Easy-nLC 1200 liquid chromatography system coupled to an Orbitrap Q-Exactive HF instrument	Thermo Fisher Scientific	
Vacuum centrifuge	Heto Lab	

Methods and Protocols

Isolation and culture of primary murine neonatal cardiomyocytes

NMRI male mice (Janvier Labs) were housed in the Central Animal Laboratory of University of Turku. The housing, upkeep, and euthanasia of animals were conducted according to Directive 2010/63/EU and under license from The Ministry of Agriculture and Forestry of Finland. The neonatal mice were sacrificed by decapitation. Freshly dissected neonatal (≤3 days of postpartum) hearts were minced and washed twice with ice-cold HBSS (Hank's balanced salt solution). The hearts were enzymatically digested with Cardiomyocyte Isolation Enzymes 1 and 2, papain, and thermolysin, according to the manufacturer's instructions, except that thermolysin was used 1:5 of its suggested volume. The samples were washed twice with ice-cold ADS buffer (Louch *et al*, 2011), mechanically agitated, and centrifuged at 900 *g* for 6 min in ADS buffer. The isolated cells were purified with a Percoll gradient, as previously described (Louch *et al*, 2011). Cell concentration and viability of cardiomyocytes were determined with TC20 Automated Cell Counter. Cells were plated on 1% gelatin-coated plates and maintained in plating medium (68% DMEM, 17% 199, 10% horse serum, 5% fetal bovine serum, pH 7.2; Louch *et al*, 2011). After 2 days, the medium was changed to serum-free maintenance medium (80% DMEM, 20% 199, pH 7.2, 5 mM Creatine, 2 mM Carnitine, 5 mM Taurine; Louch *et al*, 2011). For immunofluorescence analyses, the primary neonatal cardiomyocytes were plated in coverslips coated with 2% growth factor reduced Matrigel and cultured in plating medium. The primary cultures were sporadically tested for mycoplasma infections and infected cells were disposed.

Zebrafish husbandry

Zebrafish (*Danio rerio*) of casper strain (*roy*, *mitfa*) were housed at Zebrafish Core of Turku Bioscience Center, University of Turku and Åbo Akademi according to standard procedures (Nüsslein-Volhard & Dahm, 2002). Embryos were obtained through natural spawning in dedicated breeding tanks. After collection, the embryos were flushed and incubated in E3-medium at +28.5°C in a humidified incubator. The zebrafish embryos were anesthetized by administrating a single dose of tricaine (Ethyl 3-aminobenzoate methanesulfonate) into the culture medium at end concentration of 200 mg/l. The zebrafish embryos were euthanized under terminal anesthesia by fixation in 4% paraformaldehyde or direct homogenization using a motorized pellet pestle. The zebrafish embryos at the age (< 5dpf) used in experiments are not considered protected animals as defined by Directive 2010/63/EU. The adult zebrafish were housed and used in mating according to Directive 2010/63/EU and under license MMM/465/712-93 (Ministry of Forestry and Agriculture). The ARRIVE 2.0 reporting guideline was utilized. No statistical method was used for sample size estimation due to the high yield of embryos per spawning. The embryos were randomly allocated from one plate to different experimental groups. The group allocation was executed by a separate investigator independent of the investigators who analyzed the embryos. Underdeveloped embryos were excluded before treatment. Dead embryos were excluded before and after treatment. These exclusion criteria were set *a priori*.

Patient sample characteristics

The formalin-fixed paraffin-embedded myocardial tissue sections were acquired from Auria biobank though an application process (application number: AB20-3971). The Finnish Biobank Act (Finlex 688/2012) enables the use of biobank resources in research. The patients whose samples have been used in the study have given their consent to use their samples in research to Auria biobank. The research conforms to the principles outlined in the Declaration of Helsinki. The cohorts included myocardial samples obtained from 19 patients who underwent medical autopsy at Turku University Hospital between 2008 and 2017. The hypertrophy cohort (median age 67; 23% female) included six samples from patients with aortic valve stenosis, four samples from patients with alcoholic cardiomyopathy and three from patients with idiopathic cardiomyopathy. The control cohort (median age 48; 50% female) included six cardiac samples taken from autopsied patients with noncardiac diseases (two cases of cirrhosis, one case of metastatic pancreatic carcinoid, one case of pulmonary embolism, one case of sepsis due to *Streptococcus pneumoniae*, and one case of cholangiocarcinoma). All the cases in the control cohort were negative for cardiomyocyte hypertrophy based on a histopathological analysis. One hypertrophy sample where the mean cardiomyocyte thickness was equal to the normal controls was excluded from the analysis.

Adeno-associated virus-treated mouse samples

The adeno-associated virus (AAV)-treated mouse samples were acquired from the experiments described previously (Kivelä *et al*, 2019). Before tissue collection, mice were injected intraperitoneally with 80 mg/kg of ketamine and 10 mg/kg of xylazine and euthanized by cervical dislocation. The local committee appointed by the district of southern Finland approved the animal experiments. FELASA (Federation of European Laboratory Animal Science Associations) guidelines and recommendations were followed. All the animal procedures and experiments were performed under the

EU directive 2010/63/EU guidelines of the European parliament on the protection of animals used for scientific purposes.

Viral transduction

Lentiviral vectors were produced in HEK293T cells using a third-generation lentiviral packaging system (Dull *et al*, 1998). The HEK293T cells were cultured in DMEM supplemented with 10% FBS, 5 mM UltraGlutamine, and 1 U of penicillin and streptomycin. Cells were co-transfected overnight with pRSV-Rev, pMDLg/pRRE, pMD2.G, and pLKO.1-puromycin encoding one of the shRNA constructs. Medium was changed 24 h after transfection, and virus-containing medium was collected at 48 and 72 h and filtered. Primary cardiomyocytes were infected with the lentiviruses at a multiplicity of infection (MOI) of 1 in the presence of 8 μg/ml polybrene. The medium was changed to serum-free maintenance medium (80% DMEM, 20% 199, pH 7.2, 5 mM Creatine, 2 mM Carnitine, 5 mM Taurine; Louch *et al*, 2011) after 5 h. The cells were analyzed 24 h after infection.

Neuregulin stimulation and chemical inhibition

For western analyses, cells were stimulated with 50 ng/ml of human recombinant NRG-1β for 2 min where indicated. For real-time RT-PCR analyses, the cells were incubated with 50 ng/ml NRG-1β for 30 min. For immunofluorescence analyses of hypertrophic growth, the isolated cardiomyocytes were incubated with 50 ng/ml NRG-1β for 2 days. To inhibit signaling, isolated cardiomyocytes were treated with the ERBB inhibitor 10 μM AG 1478 for 1 h or 50 μM dynasore for 3–6 h. To analyze the effect of ERBB or dynamin inhibition to the morphology and function of the heart of embryonic zebrafish, zebrafish embryos were immersed in E3-medium supplemented with 10 μM AG 1478, 30 μM lapatinib, 30 μM gefitinib or 50 μM dynasore at 2 dpf for 2–3 days. To analyze the effect of ERBB or dynamin inhibition on downstream signaling with western analyses, zebrafish embryos at 4–5 dpf were immersed in E3-medium supplemented with 10 μM AG 1478, 30 μM lapatinib, 30 μM gefitinib or 50 μM dynasore for 1–3 h. To analyze the effect of NRG-1 on the morphology and function of the heart of embryonic zebrafish, 100 pg of recombinant human NRG-1β or control substance (0.2% BSA in PBS) was microinjected to the pericardial sac of 2 dpf zebrafish embryos and the embryos were analyzed at 4–5 dpf. To analyze the effect of NRG-1 to downstream signaling with western analysis, 100 pg of recombinant human NRG-1β with 100 mM Na_3VO_4 or control substance with 100 mM Na_3VO_4 was microinjected to the pericardial sac of 4–5 dpf zebrafish embryos and lysed after 20 min.

Immunofluorescence and immunohistochemistry

For immunofluorescence analysis of isolated cardiomyocytes, samples were fixed and permeabilized with methanol for 10–15 min at −20°C and stained with the indicated primary antibodies. To remove nonspecific binding, 3% BSA in PBS was used as a blocking agent. Primary antibodies were detected with Alexa-conjugated secondary antibodies and nuclei were visualized with DAPI. Mowiol was used for mounting. The samples were imaged with Zeiss LSM 780 confocal microscope with the 40× and 63× Zeiss C-Apochromat objectives (Numerical Aperture: 1.2).

For immunofluorescence analysis of murine cardiac cryosections, the cryosections were allowed to reach room temperature and were rehydrated in PBS for 30 min. Sections were blocked by 3% BSA in PBS and stained with anti-STAT5b for 3 h. The sections were washed three times with PBS and incubated with the secondary Alexa Fluor 488 goat anti-rabbit antibody. Actin and nuclei were visualized with Alexa Fluor 555-conjugated phalloidin and DAPI (4′,6-diamidino-2-phenylindole), respectively. Coverslips were mounted with Mowiol. The samples were imaged with Zeiss LSM 780 and 880 confocal microscopes with the 40× Zeiss C-Apochromat and the 40x Zeiss LD LCI Plan-Apochromat objectives (Numerical Aperture: 1.2).

For immunofluorescence analysis of zebrafish embryos, the embryos were fixed and permeabilized with 4% PFA and 0.2% Triton X-100 in PBS for 30 min. The embryos were washed four times with 0.2% Tween 20 in PBS and blocked with 3% BSA and 0.2% Tween 20 in PBS for 1 h. The primary and Alexa 555- or 488-conjugated secondary antibodies were incubated overnight in +4°C under gentle agitation. The embryos were washed 4 times with 0.2% Tween 20 in PBS for 30 min under gentle agitation after primary and secondary antibody incubation. The stained embryos were imaged with Zeiss LSM 780 confocal microscope with the 40× Zeiss C-Apochromat objective. The images were captured and analyzed independently by two separate investigators.

Human heart tissue sections were analyzed by immunohistochemistry in the Histology Core Facility of the Institute of Biomedicine, University of Turku. After deparaffinization and rehydration, the sections were incubated in Tris-EDTA pH 9.0 in microwave oven for 7 min with 600 W followed by 7 min with 450 W, for antigen retrieval. The sections were incubated in the presence of hydrogen peroxide to inhibit endogenous enzyme function and in normal antibody diluent to prevent nonspecific binding of proteins. The sections were stained with an automated Labvision autostainer with anti-pSTAT5 for 60 min in room temperature. Primary antibody was detected with BrightVision Goat Anti- Mouse/Rabbit IgG HRP two step detection system with horseradish peroxidase (HRP)-conjugated secondary antibodies. Slides were counterstained with Mayer's hematoxylin for 1 min at room temperature, dehydrated and mounted with Pertex. The stained section were imaged with Panoramic P1000 slide scanner. The samples were analyzed blind.

Proximity ligation assay

The proximity ligation assay of dynamin-2/ERBB4 association was performed according to the manufacturer's protocol with anti-mouse minus and anti-goat plus probes. A 1:100 dilution of primary dynamin-2 and ERBB4 antibodies was used. The primary ERBB4 antibody was omitted from the technical control.

Western analysis

The zebrafish embryos were ground with an electronic pestle into 6× Laemmli buffer and incubated at 100°C for 10 min. The primary cultures were lysed with Triton-X based lysis buffer (0.1% Triton X-100, 1 mM EDTA, 5 mM NaF, 10 mM Tris–HCl, pH 7.4, and a protease inhibitor cocktail). The protein concentration was measured with Bradford assay and adjusted, and 6× Laemmli buffer was added to the lysed samples to obtain a 1× Laemmli solution. The samples were incubated at 100°C for 5 min. After incubation, the samples were centrifuged and loaded onto SDS–PAGE gels, run, and transferred to nitrocellulose membranes. The membranes were probed with the indicated primary antibodies and IR-conjugated secondary antibodies

and imaged with the Li-COR Odyssey system. The densitometric quantitation was performed with Image Studio Lite.

RNA extraction and real-time RT-PCR

Total RNA was extracted using TRIsure RNA isolation reagent according to the manufacturer's instructions. RNA concentrations were determined using a Nanodrop spectrophotometer, and complementary DNA was synthesized with Sensifast cDNA Synthesis Kit from 1 μg of total RNA. Real-time RT–PCR analyses of gene expression were performed with 500 nM of primers, 100 nM of 5′ 6-FAM-labeled probe and TaqMan universal Master Mix II according to the manufacturer's protocol. Thermal cycling was performed with QuantStudio 12K Flex Real-Time PCR System. The relative real-time RT PCR values were determined by normalizing the C_t values of the gene of interest with the C_t values of the housekeeping genes as follows: $2^{C_t \text{ gene of interest}} - 2^{C_t \text{ housekeeping gene}}$. The C_t values of the genes of interest in isolated cardiomyocytes were normalized to the average C_t values of *B2m* and *Ppia* housekeeping genes. The C_t values of the genes of interest in cardiac tissue samples were normalized to the C_t value of the *Tpt1* gene. Some replicates were excluded due to technical concerns.

In vivo imaging of zebrafish embryos

The embryos were anesthetized with Tricaine methane-sulfonate and molded into low-melting point agarose. The fast time laps videos of embryos were taken with HC Image Software of Zeiss AxioZOOM.V16 with 1.0× PlanApo Z objective with 80× magnification. The videos were imaged and analyzed independently by two separate investigators.

CRISPR/Cas9 mediated knockdown of STAT5b in zebrafish embryos

The CRISPR/Cas9 mediated knockdown was carried out largely as described in a previous report (Hoshijima *et al*, 2019). Guide RNAs were generated by combining 5 μl of crRNAs (100 μM) and tracRNA (100 μM). Duplexes were annealed by heating to 95°C for 5 min, cooled down by 0.1°C/s to 25°C, and incubated at 25°C for 5 min. Ten microlitre of nuclease-free duplex buffer (IDT) was added to reach a final concentration of 25 μM and duplexes were stored at −20°C.

To generate crRNA:tracRNA:Cas9 complexes, 1 μl of duplex, 1.25 μl of EnGen Cas9 NLS solution, 1.75 μl H_2O, and 1 μl of phenol red solution were mixed together and incubated for 5 min at 37°C prior to injection. Next, 2.3 nl of the solution was injected into 1–4 cell stage zebrafish embryos of casper line using Nanoject II microinjector. After injection, the embryos were placed in a +28.5°C incubator in E3-medium supplemented with 1:100 Pencillin-Streptomycin mixture. At 1 dpf, dead embryos were removed and 15 μl of pronase E was added to facilitate hatching. The embryos were analyzed at 4 dpf.

Cell culture

The MDA-MB-468 and HC11 cell lines stably expressing ErbB4 JM-a and JM-b have been described before (Sundvall *et al*, 2012). The HC11 cells were cultured in RPMI supplemented with 10% FBS, 2 mM UltraGlutamine, 1 U penicillin and streptomycin, 100 ng/ml EGF, 300 ng/ml puromycin and 1:2000 insulin solution. The MCF-7 cells were cultured in RPMI supplemented with 10% FBS, 5 mM UltraGlutamine, 1 U penicillin and streptomycin, 10 nM estrogen and 1:2000 insulin solution. The MDA-MB-468 cells were cultured in DMEM supplemented with 10% FBS, 5 mM Glutamine, 1 U penicillin and streptomycin and 300 ng/ml puromycin. All cell lines were maintained at 37°C in 5% CO_2 in media. The cell lines were sporadically tested for mycoplasma infections and infected cells were disposed. No authentications were recently performed for the cell lines.

Transfection

Fugene 6 or Hilymax was used for DNA plasmid transfection in MCF-7, and Lipofectamine 2000 for siRNA transfection in MDA-MB-468 cells, as recommended by the manufacturer's protocol. DNM2 siRNAs were used at 30 nM concentration and incubated with the cells for 48 h. STAT5 siRNAs were used at 50 nM concentration and incubated with the cells for 48 h.

Immunoprecipitation

The cells were serum starved and treated where indicated with 50 ng/ml NRG-1β for 2 min before lysis with Triton-X based lysis buffer (0.1% Triton X-100, 1 mM EDTA, 5 mM NaF, 10 mM Tris–HCl, pH 7.4, and a protease inhibitor cocktail). The lysates were precleared for 1 h at 4°C with G-sepharose beads before immunoprecipitation for 3–12 h at 4°C with the indicated antibodies. The immunoprecipitates were washed seven times with 0.2% Tween 20 in PBS and eluted and denatured with incubation with 6× Laemmli buffer for 5 min at 100°C. The samples were loaded onto SDS–PAGE gels, run, and transferred to nitrocellulose membranes. The membranes were probed with the the indicated primary antibodies and HRP (horseradish peroxidase)-linked secondary antibodies. The membranes were incubated with a chemiluminescence substrate for 5 min and the light signal was captured with X-ray film.

Mass spectrometry

The cells were cross-linked with 1 mM DSP or DTPB for 2 min and quenched with 50 mM Tris–HCl pH 7.4 for 15 min at room temperature. The cross-linked cells were lysed with Triton-X based lysis buffer and precleared with 50 μl of preclear beads for 1 h at 4°C under gentle agitation. To prepare the beads for the preclearing, 160 μl of magnetic G-protein beads were blocked with 5% BSA, incubated with 8 μg mouse IgG and 8 μg of rabbit IgG for 3 h at 4°C and cross-linked with 3 mM BS3 crosslinker for 30 min at room temperature. The mixture was quenched with 50 mM Tris pH 7.5. The precleared lysate was incubated with the ErbB4 antibodies cross-linked to magnetic G-protein beads for 3 h at 4°C under gentle agitation. To prepare the ErbB4 G-protein beads, 160 μl of magnetic G-protein beads were blocked with 5% BSA, incubated with 8 μg anti-ErbB4 (HFR-1) and 8 μg anti-ErbB4 (E200) for 3 h at 4°C and cross-linked with 3 mM BS_3 crosslinker for 30 min at room temperature. The mixture was quenched with 50 mM Tris pH 7.5 for 15 min and washed 3 times with 0.1% Tween 20 in PBS. The immunoprecipitates were washed 7 times with 0.2% Tween 20 in PBS. In the first experiment, the MDA-MB-468 ErbB4 JM-a and JM-b immunoprecipitates were eluted with 0.2 M glycine (pH 2.5), methanol-cholorform precipitated and sent to Proteomics Core Laboratory in the University of Tartu for LC/MS/MS analysis with Thermo Fisher Scientific LTQ Orbitrap XL mass-spectrometer. The mass spectrometry files were analyzed with MaxQuant software. In the second experiment, the MDA-MB-468 ErbB4 JM-a and JM-b

immunoprecipitates were eluted with 6 M guanidine hydrochloride, 5 mM tris(2-carboxyethyl)phosphine, 10 mM chloroacetamide and 100 mM Tris, pH 8.5 in 95°C for 10 min. Guanidine hydrochloride was diluted to 2 M and eluted samples were digested with 1:50 (w/v) trypsin overnight at 37°C. Following digestion, the reactions were quenched with 10% trifluoroacetic acid at a final concentration of approximately 0.5% (pH ~ 2), desalted on tC18 SepPak 96-well plate, and dried by vacuum centrifugation. The mass spectrometry analyses were performed in the Turku Proteomics Facility at Turku Bioscience (University of Turku and Åbo Akademi University). The dried peptides samples were resuspended in 0.1% formic acid before analysis with mass spectrometers. The peptides were analyzed on an Easy-nLC 1200 liquid chromatography system coupled to an Orbitrap Q-Exactive HF instrument equipped with a nanoelectrospray source. Peptides were loaded on an in-house packed 100 μm × 2 cm precolumn packed with ReproSil-Pur 5 μm 200 Å C18-AQ beads using 0.1% formic acid in water (buffer A) and separated by reverse phase chromatography on a 75 μm × 15 cm analytical column packed with ReproSil-Pur 5 μm 200 Å C18-AQ beads. All separations were performed using a 40 min gradient at a flow rate of 300 nl/min. The gradient ranged from 6% buffer B (80% acetonitrile in 0.1% formic acid) to 36% buffer B in 30 min. Buffer B concentration was ramped up to 100% in 5 min, and 100% buffer B was run 5 min for washout. The DDA method consisted of a full MS scan (120,000 resolution, 3E6 automatic gain control [AGC] target, 100 ms maximum injection time, 300–1,750 m/z, profile mode), followed by data-dependent MS/MS acquisitions on the top 20 most intense precursor ions (15,000 resolution, 5E4 AGC target, 100 ms maximum injection time, 2.0 m/z isolation window, normalized collision energy = 27, centroid mode). MS/MS spectra were searched with Metamorpheus against human proteome. Proteomes contained known post-translational modifications (downloaded from Uniprot at 10.1.2021). Mass spectrometry files were calibrated, possible post-translational modifications were searched, and peptides and proteins were identified, and quantified using FlashLFQ algorithm. Cysteine carbamidomethylation (57.021463) was set as a constant modification and methionine oxidation was set as a variable modification. All other possible modifications were set using G-DPM search in Metamorpheus. Search results were filtered to a 1% FDR at PSM level. Peptides were accepted with search engine score above 5. The analyzed mass spectrometry data is provided as Dataset EV1 and EV2.

Genomic DNA and RNA isolation from zebrafish embryos

To isolate genomic DNA and RNA from zebrafish embryos, the embryos were lysed with an electronic pestle to the lysis buffer of the NucleoSpin TriPrep. The genomic DNA and RNA isolation was conducted with the NucleoSpin TriPrep kit according to the manufacturer's protocol.

Nested PCR and sequencing

For sequencing CRISPR/Cas9 edited zebrafish, the genomic DNA of the zebrafish embryos were amplified by PCR using 10 nM outer Dr. Cas9.STAT5B primers with Taq I polymerase. The PCR products from the first PCR amplification were used as a template for amplification with 10 nM inner Dr.Cas9.STAT5B primers and the PCR reactions were supplemented with 2.5 mM Mg_2Cl_2. The amplified product was Sanger sequenced.

Preparation of formalin fixed paraffin embedded samples

To prepare formalin fixed paraffin embedded (FFPE) samples to control the specificity of the pSTAT5 immunostaining, MCF-7 cells were serum starved for 12 h and treated or not with 1:2000 insulin solution for 10 min, and MDA-MB-468 cells were transfected with control or STAT5 siRNAs and serum starved for 12 h. The cells were incubated with a trypsin–EDTA solution at 37°C for 5 min to detach the cells, centrifuged for 5 min with 500 g in +4°C and washed twice with ice-cold PBS. The cells were fixed with 10% neutral buffered formalin in PBS for 20 min in room temperature and washed twice with PBS. The cells were suspended into 1.5% agarose in PBS warmed to 50°C and allowed to cool down to room temperature for 15 min. The agarose cell pellets were transferred to 70% ethanol and embedded into paraffin blocks with a standard protocol by the Histology Core Facility of the Institute of Biomedicine, University of Turku. Five μm sections from the blocks were stained as the FFPE myocardial tissue sections from patients.

Image analysis

The area of isolated cardiomyocytes and zebrafish embryo ventricles, and the thickness of ventricles was measured with Fiji. The ejection fraction of zebrafish ventricle was determined by measuring the average width of the ventricle at systole and diastole with Fiji and fitting the values to the simplified Quinones equation: $\left(\mathrm{EDD}^2-\mathrm{ESD}^2\right)/\mathrm{EDD}^2 \times 100\% + 10\%$. The ventricular width, measured from outer margins of the myocardium, at diastole and at systole was used as the end-diastolic dimension (EDD) and end-systolic dimension (ESD), respectively. The amount of PLA signals was measured with the particle analyzer function of Fiji and the location of PLA signals was analyzed with SpatTrack. The colocalization of immunofluorescence signals was measured with the algorithm of Villalta *et al*, 2011. Four colocalization measures (Pearson's correlation, Manders overlap, M1/M2, k1/k2) were produced of which $k1/k2$ ($k1 = \sum(S_1 \times S_2)/\sum(S_1)$ and $k2 = \sum(S_1 \times S_2)/\sum(S_2)$, where S_1 and S_2 are the intensity of the signal from channel 1 and 2, respectively) is visualized in the images. The relative intensity of the DAB staining was measured from color deconvoluted images with Fiji. The average intensity in the cardiomyocyte nuclei to cardiomyocyte cytosol (background) was used. The intensity of immunofluorescence signal was measured with Fiji.

Data and statistical analyses

Matlab R2016a and Graph Pad Prism 8.4.2 were used for statistical analysis. The normality and homoscedasticity of each dataset was tested with Shapiro–Wilkis, Kolmogorov–Smirnov, Bartlett's and Brown–Forsythe test and parametric, parametric testing with variance correction or nonparametric testing was chosen accordingly. All data combined from independent experiments were median normalized except for the data in Fig 1J. The data in 1J were normalized to the range to fit the combined data into a normal distribution. The transcriptome datasets of subjects with pathological hypertrophy and control subjects were downloaded from the Gene Expression Omnibus database (Edgar *et al*, 2002; Barrett *et al*, 2013). The principle component analysis of the pre-existing datasets was performed with R in RStudio. The statistical significance of the categorization of the dimensionality-reduced values was calculated by estimating an empirical probability distribution for the relative

distance and drawing the cumulative probability from the corresponding cumulative probability function. The relative distance was determined by the sum of all Euclidian distances within the category divided by the sum of all Euclidian distances between categories. The empirical probability distribution was simulated by drawing 10,000 random gene sets of same size from the dataset, subjecting the gene sets to principal component analysis and calculating the relative distance between the categories of the dimensionality reduced values. The schematic figures were created with biorender.com.

Data availability

The datasets produced in this study are available in the following databases:
The Mass spectrometry derived interactome data: ProteomeXchange Consortium (Deutsch *et al*, 2023) via the PRIDE (Perez-Riverol *et al*, 2022) partner repository PXD040166 (https://www.ebi.ac.uk/pride/archive/projects/PXD040166).

Expanded View for this article is available online.

Acknowledgments
We thank Maria Tuominen, Mika Savisalo, Nea Konttinen, Merja Lakkisto, Minna Santanen, Julia Palosara and Sinikka Kollanus for skillful technical assistance, and Riku Kiviranta and his laboratory for providing research material. Turku Doctoral Program of Molecular Medicine is acknowledged for excellent doctoral training and funding. The Auria biobank is acknowledged for providing patient samples. We acknowledge the Cell Imaging Core, Proteomics Core, Zebrafish Core and Finnish Functional Genomics Centre (Turku Bioscience Centre, University of Turku and Åbo Akademi University) all supported by Biocenter Finland and Histology Core Facility of the Institute of Biomedicine, University of Turku for their excellent service. The Proteomics Core Laboratory in the University of Tartu is acknowledged for their proteomics services. This work was financially supported by the Academy of Finland, Cancer Foundation Finland, the Sigrid Juselius Foundation, the Turku University Central Hospital, the Turku University Foundation, Orion Research Foundation, K. Albin Johansson's Foundation, the Cancer Society of Southwestern Finland, the Maud Kuistila memorial Foundation, Aarne Koskelo Foundation, Paulo Foundation, Emil Aaltonen Foundation, the Finnish Foundation for Cardiovascular Research, Paavo Nurmi Foundation, Finnish Cultural Foundation and the Varsinais-Suomi Regional Fund of the Finnish Cultural Foundation.

Author contributions
Katri Vaparanta: Conceptualization; resources; data curation; formal analysis; funding acquisition; validation; investigation; visualization; methodology; writing – original draft; project administration; writing – review and editing. **Anne Jokilammi:** Validation; investigation; methodology; writing – review and editing. **Ilkka Paatero:** Resources; investigation; methodology; writing – review and editing. **Johannes A Merilahti:** Data curation; investigation; writing – review and editing. **Juho Heliste:** Methodology; writing – review and editing. **Karthik Amudhala Hemanthakumar:** Resources. **Riikka Kivelä:** Resources; writing – review and editing. **Kari Alitalo:** Resources. **Pekka Taimen:** Resources; investigation; methodology; writing – review and editing. **Klaus Elenius:** Conceptualization; supervision; funding acquisition; visualization; writing – original draft; writing – review and editing.

Disclosure and competing interests statement
KE has ownership interest in Abomics, Novo Nordisk, Orion, and Roche. JH declares competing financial interests, including direct investments and a role as a medical advisor in Abomics Oy. PT reports personal fees from Roche, AstraZeneca, Bayer and MSD and non-financial support from MSD, all outside the described work. The other authors declare no conflict of interest.

References

Anderson NG, Ahmad T, Chan K, Dobson R, Bundred NJ (2001) ZD1839 (Iressa), a novel epidermal growth factor receptor (EGFR) tyrosine kinase inhibitor, potently inhibits the growth of EGFR-positive cancer cell lines with or without erbB2 overexpression. *Int J Cancer* 94: 774–782

Baliga RR, Pimental DR, Zhao YY, Simmons WW, Marchionni MA, Sawyer DB, Kelly RA (1999) NRG-1-induced cardiomyocyte hypertrophy. Role of PI-3-kinase, p70(S6K), and MEK-MAPK-RSK. *Am J Physiol* 277: H2026–H2037

Barrett T, Wilhite SE, Ledoux P, Evangelista C, Kim IF, Tomashevsky M, Marshall KA, Phillippy KH, Sherman PM, Holko M *et al* (2013) NCBI GENE EXPRESSION OMNIBUS: archive for functional genomics data sets–update. *Nucleic Acids Res* 41: D991–D995

Basham B, Sathe M, Grein J, McClanahan T, D'Andrea A, Lees E, Rascle A (2008) *In vivo* identification of novel STAT5 target genes. *Nucleic Acids Res* 36: 3802–3818

Bersell K, Arab S, Haring B, Kühn B (2009) Neuregulin1/ErbB4 signaling induces cardiomyocyte proliferation and repair of heart injury. *Cell* 138: 257–270

Bisping E, Ikeda S, Kong S, Tarnavski O, Bodyak N, McMullen JR, Rajagopal S, Son JK, Ma Q, Springer Z *et al* (2006) Gene Expression Omnibus GSE5500 (https://www.ncbi.nlm.nih.gov/geo/query/acc.cgi?acc=GSE5500). [DATASET]

Bongiovanni C, Sacchi F, Da PS, Pantano E, Miano C, Morelli MB, D'uva G (2021) Reawakening the intrinsic cardiac regenerative potential: molecular strategies to boost dedifferentiation and proliferation of endogenous cardiomyocytes. *Front Cardiovasc Med* 8: 750604

Cai MX, Shi XC, Chen T, Tan ZN, Lin QQ, Du SJ, Tian ZJ (2016) Exercise training activates neuregulin 1/ErbB signaling and promotes cardiac repair in a rat myocardial infarction model. *Life Sci* 149: 1–9

Chen H, Jing XY, Shen YJ, Wang TL, Ou C, Lu SF, Cai Y, Li Q, Chen X, Ding YJ *et al* (2018) Stat5-dependent cardioprotection in late remote ischaemia preconditioning. *Cardiovasc Res* 114: 679–689

Cohen JE, Purcell BP, MacArthur JW, Mu A, Shudo Y, Patel JB, Brusalis CM, Trubelja A, Fairman AS, Edwards BB *et al* (2014) A bioengineered hydrogel system enables targeted and sustained intramyocardial delivery of neuregulin, activating the cardiomyocyte cell cycle and enhancing ventricular function in a murine model of ischemic cardiomyopathy. *Circ Hear Fail* 7: 619–626

Cox J, Mann M (2008) MaxQuant enables high peptide identification rates, individualized p.p.b.-range mass accuracies and proteome-wide protein quantification. *Nat Biotechnol* 26: 1367–1372

Crone SA, Zhao YY, Fan L, Gu Y, Minamisawa S, Liu Y, Peterson KL, Chen J, Kahn R, Condorelli G *et al* (2002) ErbB2 is essential in the prevention of dilated cardiomyopathy. *Nat Med* 8: 459–465

De Keulenaer GW, Feyen E, Dugaucquier L, Shakeri H, Shchendrygina A, Belenkov YN, Brink M, Vermeulen Z, Segers VFM (2019) Mechanisms of the multitasking endothelial protein NRG-1 as a compensatory factor during chronic heart failure. *Circ Heart Fail* 12: 6288

Delaughter MC, Taffet GE, Fiorotto ML, Entman ML, Schwartz RJ (1999) Local insulin-like growth factor I expression induces physiologic, then pathologic, cardiac hypertrophy in transgenic mice. *FASEB J* 13: 1923–1929

Deutsch EW, Bandeira N, Perez-Riverol Y, Sharma V, Carver JJ, Mendoza L, Kundu DJ, Wang S, Bandla C, Kamatchinathan S *et al* (2023) The ProteomeXchange consortium at 10 years: 2023 update. *Nucleic Acids Res* 51: D1539–D1548

Dull T, Zufferey R, Kelly M, Mandel RJ, Nguyen M, Trono D, Naldini L (1998) A third-generation lentivirus vector with a conditional packaging system. *J Virol* 72: 8463–8471

D'uva G, Aharonov A, Lauriola M, Kain D, Yahalom-Ronen Y, Carvalho S, Weisinger K, Bassat E, Rajchman D, Yifa O *et al* (2015) ERBB2 triggers mammalian heart regeneration by promoting cardiomyocyte dedifferentiation and proliferation. *Nat Cell Biol* 17: 627–638

Edgar R, Domrachev M, Lash AE (2002) Gene Expression Omnibus: NCBI gene expression and hybridization array data repository. *Nucleic Acids Res* 30: 207–210

Egeblad M, Mortensen OH, Van Kempen LCLT, Jäättelä M (2001) BIBX1382BS, but not AG1478 or PD153035, inhibits the ErbB kinases at different concentrations in intact cells. *Biochem Biophys Res Commun* 281: 25–31

Elenius K, Corfas G, Paul S, Choi CJ, Rio C, Plowman GD, Klagsbrun M (1997) A novel Juxtamembrane domain isoform of HER4/ErbB4: isoform-specific tissue distribution and differential processing in response to phorbol ester. *J Biol Chem* 272: 26761–26768

Fukazawa R, Miller TA, Kuramochi Y, Frantz S, Kim Y-D, Marchionni MA, Kelly RA, Sawyer DB (2003) Neuregulin-1 protects ventricular myocytes from anthracycline-induced apoptosis via erbB4-dependent activation of PI3-kinase/Akt. *J Mol Cell Cardiol* 35: 1473–1479

Gallo S, Vitacolonna A, Bonzano A, Comoglio P, Crepaldi T (2019) ERK: a key player in the pathophysiology of cardiac hypertrophy. *Int J Mol Sci* 20: 2164

Gao R, Zhang J, Cheng L, Wu X, Dong W, Yang X, Li T, Liu X, Xu Y, Li X *et al* (2010) A phase II, randomized, double-blind, multicenter, based on standard therapy, placebo-controlled study of the efficacy and safety of recombinant human neuregulin-1 in patients with chronic heart failure. *J Am Coll Cardiol* 55: 1907–1914

Gao R, Zhang J, Liu H, Wang L, Pang X, Fu L, Meng F, Zhou M (2018) A Phase III, randomized, double-blind, multicenter, placebo-controlled study of the efficacy and safety of neucardin in patients with chronic heart failure. *J Am Coll Cardiol* 71: A668

García-Rivello H, Taranda J, Said M, Cabeza-Meckert P, Vila-Petroff M, Scaglione J, Ghio S, Chen J, Lai C, Laguens RP *et al* (2005) Dilated cardiomyopathy in Erb-b4-deficient ventricular muscle. *Am J Physiol* 289: H1153–H1160

Gassmann M, Casagranda F, Orioli D, Simon H, Lai C, Klein R, Lemke G (1995) Aberrant neural and cardiac development in mice lacking the ErbB4 neuregulin receptor. *Nature* 378: 390–394

Gemberling M, Karra R, Dickson AL, Poss KD (2015) Nrg1 is an injury-induced cardiomyocyte mitogen for the endogenous heart regeneration program in zebrafish. *Elife* 4: e05871

Hebl VB, Bos JM, Oberg AL, Sun Z, Herman DS, Teekakirikul P, Seidman JG, Seidman CE, dos Remedios CG, Schaff HV *et al* (2012) Gene Expression Omnibus GSE36961 (https://www.ncbi.nlm.nih.gov/geo/query/acc.cgi?acc=GSE36961). [DATASET]

Hedhli N, Huang Q, Kalinowski A, Palmeri M, Hu X, Russell RR, Russell KS (2011) Endothelium-derived neuregulin protects the heart against ischemic injury. *Circulation* 123: 2254–2262

Heusch G, Musiolik J, Kottenberg E, Peters J, Jakob H, Thielmann M (2012) STAT5 activation and cardioprotection by remote ischemic preconditioning in HumansNovelty and significance. *Circ Res* 110: 111–115

Hirai M, Arita Y, McGlade CJ, Lee KF, Chen J, Evans SM (2017) Adaptor proteins NUMB and NUMBL promote cell cycle withdrawal by targeting ERBB2 for degradation. *J Clin Invest* 127: 569–582

Hoshijima K, Jurynec MJ, Klatt Shaw D, Jacobi AM, Behlke MA, Grunwald DJ (2019) Highly efficient CRISPR-Cas9-based methods for generating deletion mutations and F0 embryos that lack Gene function in zebrafish. *Dev Cell* 51: 645–657.e4

Huang CY, Lin YC, Hsiao WY, Liao FH, Huang PY, Tan TH (2012) DUSP4 deficiency enhances CD25 expression and CD4+ T-cell proliferation without impeding T-cell development. *Eur J Immunol* 42: 476–488

Jabbour A, Hayward CS, Keogh AM, Kotlyar E, McCrohon JA, England JF, Amor R, Liu X, Li XY, Zhou MD *et al* (2011) Parenteral administration of recombinant human neuregulin-1 to patients with stable chronic heart failure produces favourable acute and chronic haemodynamic responses. *Eur J Heart Fail* 13: 83–92

Jie B, Zhang X, Wu X, Xin Y, Liu Y, Guo Y (2012) Neuregulin-1 suppresses cardiomyocyte apoptosis by activating PI3K/Akt and inhibiting mitochondrial permeability transition pore. *Mol Cell Biochem* 370: 35–43

Jin G, Wang L, Ma J (2022) Inhibiting STAT5 significantly attenuated ang II-induced cardiac dysfunction and inflammation. *Eur J Pharmacol* 915: 174689

Kehat I, Davis J, Tiburcy M, Accornero F, Saba-El-Leil MK, Maillet M, York AJ, Lorenz JN, Zimmermann WH, Meloche S *et al* (2011) ERK1/2 regulate the balance between eccentric and concentric cardiac growth. *Circ Res* 108: 176–183

Kimura A, Ishida Y, Furuta M, Nosaka M, Kuninaka Y, Taruya A, Mukaida N, Kondo T (2018) Protective roles of interferon-γ in cardiac hypertrophy induced by sustained pressure overload. *J Am Hear Assoc Cardiovasc Cerebrovasc Dis* 7: e008145

Kivelä R, Hemanthakumar KA, Vaparanta K, Robciuc M, Izumiya Y, Kidoya H, Takakura N, Peng X, Sawyer DB, Elenius K *et al* (2019) Endothelial cells regulate physiological cardiomyocyte growth via VEGFR2-mediated paracrine signaling. *Circulation* 139: 2570–2584

Komamura K (2017) Recombinant insulin-like growth factor-1 improves cardiac function and symptoms in the patients on the waiting list for heart transplantation with end-stage dilated cardiomyopathy. *Eur Heart J* 38: ehx502.P1105

Kuramochi Y, Guo X, Sawyer DB (2006) Neuregulin activates erbB2-dependent src/FAK signaling and cytoskeletal remodeling in isolated adult rat cardiac myocytes. *J Mol Cell Cardiol* 41: 228–235

Lai L, Martin O, Leone TC, Kelly DP (2014) Gene Expression Omnibus GSE56348 (https://www.ncbi.nlm.nih.gov/geo/query/acc.cgi?acc=GSE56348). [DATASET]

Lee KF, Simon H, Chen H, Bates B, Hung MC, Hauser C (1995) Requirement for neuregulin receptor erbB2 in neural and cardiac development. *Nature* 378: 394–398

Lemmens K, Segers VFM, Demolder M, De Keulenaer GW (2006) Role of Neuregulin-1/ErbB2 signaling in endothelium-cardiomyocyte cross-talk. *J Biol Chem* 281: 19469–19477

Li J, Zhang DS, Ye JC, Li CM, Qi M, Liang DD, Xu XR, Xu L, Liu Y, Zhang H *et al* (2013) Dynamin-2 mediates heart failure by modulating Ca^{2+}–dependent cardiomyocyte apoptosis. *Int J Cardiol* 168: 2109–2119

Liu X, Gu X, Li Z, Li X, Li H, Chang J, Chen P, Jin J, Xi B, Chen D *et al* (2006) Neuregulin-1/erbB-activation improves cardiac function and survival in models of ischemic, dilated, and viral cardiomyopathy. *J Am Coll Cardiol* 48: 1438–1447

Liu J, Bressan M, Hassel D, Huisken J, Staudt D, Kikuchi K, Poss KD, Mikawa T, Stainier DYR (2010) A dual role for ErbB2 signaling in cardiac trabeculation. *Development* 137: 3867–3875

Lock MC, Tellam RL, Botting KJ, Wang KCW, Selvanayagam JB, Brooks DA, Seed M, Morrison JL (2018) The role of miRNA regulation in fetal

cardiomyocytes, cardiac maturation and the risk of heart disease in adults. *J Physiol* 596: 5625–5640

Lord JD, McIntosh BC, Greenberg PD, Nelson BH (2000) The IL-2 receptor promotes lymphocyte proliferation and induction of the c-myc, bcl-2, and bcl-x genes through the trans-activation domain of Stat5. *J Immunol* 164: 2533–2541

Louch WE, Sheehan KA, Wolska BM (2011) Methods in cardiomyocyte isolation, culture, and gene transfer. *J Mol Cell Cardiol* 51: 288–298

Lund FW, Jensen MLV, Christensen T, Nielsen GK, Heegaard CW, Wüstner D (2014) SpatTrack: an imaging toolbox for analysis of vesicle motility and distribution in living cells. *Traffic* 15: 1406–1429

Maatta JA, Sundvall M, Junttila TT, Peri L, Laine VJO, Isola J, Egeblad M, Elenius K (2005) Proteolytic cleavage and phosphorylation of a tumor-associated ErbB4 isoform promote ligand-independent survival and cancer cell growth. *Mol Biol Cell* 17: 67–79

Margulies KB, Cappola TP (2019) Gene Expression Omnibus GSE141910 (https://www.ncbi.nlm.nih.gov/geo/query/acc.cgi?acc=GSE141910). [DATASET]

Martens N, Uzan G, Wery M, Hooghe R, Hooghe-Peters EL, Gertler A (2005) Suppressor of cytokine signaling 7 inhibits prolactin, growth hormone, and leptin signaling by interacting with STAT5 or STAT3 and attenuating their nuclear translocation. *J Biol Chem* 280: 13817–13823

Mendes-Ferreira P, De Keulenaer GW, Leite-Moreira AF, Brás-Silva C (2013) Therapeutic potential of neuregulin-1 in cardiovascular disease. *Drug Discov Today* 18: 836–842

Meyer D, Birchmeier C (1995) Multiple essential functions of neuregulin in development. *Nature* 378: 386–390

Millikin RJ, Solntsev SK, Shortreed MR, Smith LM (2018) Ultrafast peptide label-free quantification with FlashLFQ. *J Proteome Res* 17: 386–391

Montero JC, Yuste L, Díaz-Rodríguez E, Esparís-Ogando A, Pandiella A (2000) Differential shedding of transmembrane neuregulin isoforms by the tumor necrosis factor-α-converting enzyme. *Mol Cell Neurosci* 16: 631–648

Nakajima H, Brindle PK, Handa M, Ihle JN (2001) Functional interaction of STAT5 and nuclear receptor co-repressor SMRT: implications in negative regulation of STAT5-dependent transcription. *EMBO J* 20: 6836–6844

Nakamura M, Sadoshima J (2018) Mechanisms of physiological and pathological cardiac hypertrophy. *Nat Rev Cardiol* 15: 387–407

Nosaka T, Kawashima T, Misawa K, Ikuta K, Mui ALF, Kitamura T (1999) STAT5 as a molecular regulator of proliferation, differentiation and apoptosis in hematopoietic cells. *EMBO J* 18: 4754–4765

Nüsslein-Volhard C, Dahm R (2002) *Zebrafish: a practical approach*, 1st edn. Oxford: Oxford University Press

Odiete O, Hill MF, Sawyer DB (2012) Neuregulin in cardiovascular development and disease. *Circ Res* 111: 1376–1385

Özcelik C, Erdmann B, Pilz B, Wettschureck N, Britsch S, Hübner N, Chien KR, Birchmeier C, Garratt AN (2002) Conditional mutation of the ErbB2 (HER2) receptor in cardiomyocytes leads to dilated cardiomyopathy. *Proc Natl Acad Sci USA* 99: 8880–8885

Papatheodorou I, Moreno P, Manning J, Fuentes AMP, Gene Expression Omnibusrge N, Fexova S, Fonseca NA, Füllgrabe A, Green M, Huang N *et al* (2020) Expression atlas update: from tissues to single cells. *Nucleic Acids Res* 48: D77–D83

Paul A, Schinke M, Brown J, Riggi LE, Izumo S, Bartunek J, Allen P, M T (2004) Gene Expression Omnibus GSE1145 (https://www.ncbi.nlm.nih.gov/geo/query/acc.cgi?acc=GSE1145) [DATASET]

Peng Y, Zhou B, Wang Y, Chen Y, Li H, Song Y, Zhang L, Rao L (2012) Association between polymorphisms in the signal transducer and activator of transcription and dilated cardiomyopathy in the Chinese Han population. *Mol Cell Biochem* 360: 197–203

Pentassuglia L, Heim P, Lebboukh S, Morandi C, Xu L, Brink M (2016) Neuregulin-1β promotes glucose uptake via PI3K/Akt in neonatal rat cardiomyocytes. *Am J Physiol Endocrinol Metab* 310: E782–E794

Perez-Riverol Y, Bai J, Bandla C, García-Seisdedos D, Hewapathirana S, Kamatchinathan S, Kundu DJ, Prakash A, Frericks-Zipper A, Eisenacher M *et al* (2022) The PRIDE database resources in 2022: a hub for mass spectrometry-based proteomics evidences. *Nucleic Acids Res* 50: D543–D552

Plowman GD, Green JM, Culouscou JM, Carlton GW, Rothwell VM, Buckley S (1993) Heregulin induces tyrosine phosphorylation of HER4/p180erbB4. *Nature* 366: 473–475

Poss KD, Wilson LG, Keating MT (2002) Heart regeneration in zebrafish. *Science* 298: 2188–2190

R Core Team (2017) *R: a language and environment for statistical computing*. Vienna, Austria: R Foundation for Statistical Computing (www.R-project.org/)

Rasouli SJ, Stainier DYR (2017) Regulation of cardiomyocyte behavior in zebrafish trabeculation by neuregulin 2a signaling. *Nat Commun* 81: 1–11

Rigacci S, Guidotti V, Parri M, Berti A (2008) Modulation of STAT5 interaction with LMW-PTP during early megakaryocyte differentiation. *Biochemistry* 47: 1482–1489

Rohrbach S, Yan X, Weinberg EO, Hasan F, Bartunek J, Marchionni MA, Lorell BH (1999) Neuregulin in cardiac hypertrophy in rats with aortic stenosis. *Circulation* 100: 407–412

Rohrbach S, Muller-Werdan U, Werdan K, Koch S, Gellerich NF, Holtz J (2005a) Apoptosis-modulating interaction of the neuregulin/erbB pathway with antracyclines in regulating Bcl-xS and Bcl-xL in cardiomyocytes. *J Mol Cell Cardiol* 38: 485–493

Rohrbach S, Niemann B, Silber RE, Holtz J (2005b) Neuregulin receptors erbB2 and erbB4in failing human myocardium. Depressed expression and attenuated activation. *Basic Res Cardiol* 100: 240–249

Romano N, Ceci M (2020) Are microRNAs responsible for cardiac hypertrophy in fish and mammals? What we can learn in the activation process in a zebrafish *ex vivo* model. *Biochim Biophys Acta Mol Basis Dis* 1866: 165896

Rotwein P (2012) Mapping the growth hormone – Stat5b – IGF-I transcriptional circuit. *Trends Endocrinol Metab* 23: 186–193

RStudio team (2019) *RStudio: integrated development for R*. Boston, MA: RStudio, PBC. (https://www.posit.co)

Samsa LA, Ito CE, Brown DR, Qian L, Liu J (2016) IgG-containing isoforms of Neuregulin-1 are dispensable for cardiac trabeculation in zebrafish. *PLoS One* 11: e0166734

Sawyer DB, Zuppinger C, Miller TA, Eppenberger HM, Suter TM (2002) Modulation of anthracycline-induced myofibrillar disarray in rat ventricular myocytes by neuregulin-1β and anti-erbB2. *Circulation* 105: 1551–1554

Schindelin J, Arganda-Carreras I, Frise E, Kaynig V, Longair M, Pietzsch T, Preibisch S, Rueden C, Saalfeld S, Schmid B *et al* (2012) Fiji: an open-source platform for biological-image analysis. *Nat Methods* 9: 676–682

Sefat-E-Khuda YM, Xing Y, Shimasaki T, Takeya M, Kuwahara K, Sakaguchi N (2004) The Sac3 homologue shd1 is involved in mitotic progression in mammalian cells. *J Biol Chem* 279: 46182–46190

Smeets P, Vogels-van den Bosch H, Willemsen P, Stassen A, Ayoubi T, van der Vusse G, van Bilsen M (2008) Gene Expression Omnibus GSE12337 (https://www.ncbi.nlm.nih.gov/geo/query/acc.cgi?acc=GSE12337). [DATASET]

Solntsev SK, Shortreed MR, Frey BL, Smith LM (2018) Enhanced global post-translational modification discovery with MetaMorpheus. *J Proteome Res* 17: 1844–1851

Sundvall M, Korhonen A, Vaparanta K, Anckar J, Halkilahti K, Salah Z, Aqeilan RI, Palvimo JJ, Sistonen L, Elenius K (2012) Protein inhibitor of activated STAT3 (PIAS3) protein promotes SUMOylation and nuclear sequestration of the intracellular domain of ErbB4 protein. *J Biol Chem* 287: 23216–23226

Vaparanta K, Jokilammi A, Tamirat M, Merilahti JAM, Salokas K, Varjosalo M, Ivaska J, Johnson MS, Elenius K (2022) An extracellular receptor tyrosine kinase motif orchestrating intracellular STAT activation. *Nat Commun* 13: 6953

Villalta JI, Galli S, Iacaruso MF, Antico Arciuch VG, Poderoso JJ, Jares-Erijman EA, Pietrasanta LI (2011) New algorithm to determine true colocalization in combination with image restoration and time-lapse confocal microscopy to map kinases in mitochondria. *PLoS One* 6: e19031

Wang Z, Chan HW, Gambarotta G, Smith NJ, Purdue BW, Pennisi DJ, Porrello ER, O'Brien SL, Reichelt ME, Thomas WG *et al* (2021) Stimulation of the four isoforms of receptor tyrosine kinase ErbB4, but not ErbB1, confers cardiomyocyte hypertrophy. *J Cell Physiol* 236: 8160–8170

Welch S, Plank D, Witt S, Glascock B, Schaefer E, Chimenti S, Andreoli AM, Limana F, Leri A, Kajstura J *et al* (2002) Cardiac-specific IGF-1 expression attenuates dilated cardiomyopathy in tropomodulin-overexpressing transgenic mice. *Circ Res* 90: 641–648

White RM, Sessa A, Burke C, Bowman T, LeBlanc J, Ceol C, Bourque C, Dovey M, Goessling W, Burns CE *et al* (2008) Transparent adult zebrafish as a tool for in vivo transplantation analysis. *Cell Stem Cell* 2: 183–189

Wu Q, Wang T, Chen S, Zhou Q, Li H, Hu N, Feng Y, Dong N, Yao S, Xia Z (2017) Cardiac protective effects of remote ischaemic preconditioning in children undergoing tetralogy of fallot repair surgery: a randomized controlled trial. *Eur Heart J* 105: 151–154

Xia W, Mullin RJ, Keith BR, Liu LH, Ma H, Rusnak DW, Owens G, Alligood KJ, Spector NL (2002) Anti-tumor activity of GW572016: a dual tyrosine kinase inhibitor blocks EGF activation of EGFR/erbB2 and downstream Erk1/2 and AKT pathways. *Oncogene* 2141: 6255–6263

Yu CL, Jin YJ, Burakoff SJ (2000) Cytosolic tyrosine dephosphorylation of STAT5: Potential Role Of SHP-2 in STAT5 regulation. *J Biol Chem* 275: 599–604

Yu JH, Zhu BM, Wickre M, Riedlinger G, Chen W, Hosui A, Robinson GW, Hennighausen L (2010) The transcription factors STAT5A and STAT5B negatively regulate cell proliferation through the activation of Cdkn2b and Cdkn1a expression. *Hepatology* 52: 1808–1818

Zensun Sci. & Tech. Co., Ltd (2018) Survival study of the recombinant human neuregulin-1β in subjects with chronic heart failure. ClinicalTrials.gov NCT03388539. https://clinicaltrials.gov/ct2/show/NCT03388593

Zhao YY, Sawyer DR, Baliga RR, Opel DJ, Han X, Marchionni MA, Kelly RA (1998) Neuregulins promote survival and growth of cardiac myocytes. Persistence of ErbB2 and ErbB4 expression in neonatal and adult ventricular myocytes. *J Biol Chem* 273: 10261–10269

Zhong W, Mao S, Tobis S, Angelis E, Jordan MC, Roos KP, Fishbein MC, De Alborán IM, MacLellan WR (2006) Hypertrophic growth in cardiac myocytes is mediated by Myc through a cyclin D2-dependent pathway. *EMBO J* 25: 3869–3879